MITRE

Sponsor: NIST
Dept. No.: P833
Contract No.: 1331L523D130S0003
Project No.: 101417.15.201.0252.BA0

Bedford, MA

MTR250410
MITRE TECHNICAL REPORT

Spectrum Monitoring Sensor for Citizens Broadband Radio Service Sharing Ecosystem Assessment

Authors:

Mark A. Krangle
Elyssa F. Kaplan
Dr. Joe Mruk

Project Manager:

Dr. Keith Hartley

December 2025

Approved By

15 December 2025

Christian Neubauer
Department Manager, P833

Date

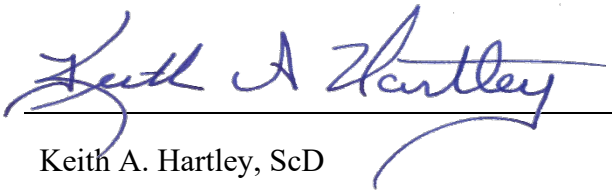

15 December 2025

Keith A. Hartley, ScD
Project Leader, N112

Date

Disclaimer

References to specific commercial entities, products, or equipment in this document are solely for the purpose of describing an experimental sensor. Such references do not constitute an endorsement or recommendation by The MITRE Corporation, nor do they imply that the identified products or equipment are the only or best options available. While reasonable efforts have been made to ensure the accuracy of the design documentation, MITRE makes no warranties, expressed or implied, regarding the completeness or reliability of the information provided. Use of this information is at your own risk.

Abstract

This report presents the design and implementation of the Citizens Broadband Radio Service (CBRS) Sharing Ecosystem Assessment (SEA) sensor. The sensor was developed to enable a National Advanced Spectrum and Communications Test Network (NASCTN) study examining the effectiveness of a new spectrum sharing methodology in the 3550 MHz to 3700 MHz CBRS band. Deployed in areas where incumbent users may be present, a network of these CBRS SEA sensors collects valuable data to assess spectrum usage and evaluate this new approach to spectrum sharing.

Executive Summary

This report describes the development of the Citizens Broadband Radio Service (CBRS) Sharing Ecosystem Assessment (SEA) sensor. The sensor was developed to enable a National Advanced Spectrum and Communications Test Network (NASCTN) study examining the effectiveness of a new spectrum sharing methodology in the 3550 MHz to 3700 MHz CBRS band. This portion of the radio frequency (RF) spectrum, historically reserved for military systems (most notably a U.S. Navy radar system) and commercial satellite ground stations, is now shared with both commercial and private entities for 4G long-term evolution (LTE), 5G, and various other communications networks following a rule change authorized by the Federal Communications Commission (FCC) in 2020. A network of CBRS SEA sensors, deployed in areas where incumbent Navy radar systems may be present, collects valuable data to assess spectrum usage and evaluate this new approach to spectrum sharing.

The SEA sensor features a modular design with separate preselector and signal processing unit (SPU) assemblies, optimizing RF performance and enabling flexible installation to adapt to various deployment site conditions. It allows for up to two external antennas, allowing both omnidirectional and directional measurements. The sensor incorporates a custom preselector filter, designed to balance measurement frequency coverage with protection from strong 5G emissions in the adjacent band. It also includes a built-in noise source for periodic self-calibration, to ensure accuracy and long-term measurement stability. The sensor is housed in sealed, weatherproof enclosures with integrated temperature control to ensure reliable operation in potentially harsh environmental conditions. At the time of this report's publication sensors have been deployed at various sites for a total of nearly 4000 sensor days, and they were operational more than 98% of that time.

This report presents a comprehensive overview of the CBRS SEA sensor, including detailed descriptions of its design and implementation, the rationale behind key design decisions, and system test results that demonstrate the sensor's performance and operational readiness, confirming its suitability for collecting accurate RF data in support of the NASCTN study.

Acknowledgments

While The MITRE Corporation served as the lead developer of the SEA sensor, its design is the result of a highly collaborative effort among members of the National Advanced Spectrum and Communications Test Network (NASCTN) team. Many individuals contributed to the design in various ways, including shaping the architecture, recommending and evaluating components, and assessing system performance. The authors gratefully acknowledge these individuals for their valuable contributions:

National Institute of Standards and Technology (NIST)

Duncan McGillivray

Aric Sanders

Keith Forsyth

Stephen Segro[1]

Dazhen Gu

Thao Nguyen

National Telecommunications and Information Administration (NTIA)

Todd Schumann

Douglas Boulware

Anthony Romaniello[1]

National Aeronautics and Space Administration (NASA)

Lee Joyce

Furthermore, the authors wish to recognize several MITRE staff members for their extensive support in the design, assembly, testing, and deployment of the sensors. Their efforts and dedication were essential to the success of this project.

Sandy Vergados

Steve Hall

Brian Chandonnet

Geoff Hamshar

Rob Scheeler[1]

[1] Former employee at the time of publication

Table of Contents

Approved By ..... **ii**
Disclaimer ..... **iii**
Abstract ..... **iv**
Executive Summary ..... **v**
Acknowledgments ..... **vi**
Table of Contents ..... **vii**
List of Figures ..... **viii**
List of Tables ..... **x**
1 Introduction **1-1**
2 Sensor Overview **2-1**
2.1 RF System 2-1
2.1.1 Omnidirectional Antenna 2-4
2.1.2 Directional Antenna 2-4
2.1.3 Bandpass Filter 2-5
2.1.4 Limiter 2-6
2.1.5 Low Noise Amplifier 2-7
2.1.6 Gain Block Amplifier 2-9
2.1.7 Real-Time Spectrum Analyzer 2-9
2.1.8 Embedded Computer 2-15
3 Sensor Implementation **3-1**
3.1 Detailed Design Documentation 3-2
3.2 Preselector Assembly 3-2
3.2.1 Preselector Thermal Testing 3-7
3.3 SPU Assembly 3-9
3.3.1 SPU Thermal Control and Testing 3-17
4 System Measurements **4-1**
4.1 Power Consumption 4-1
4.2 Gain and Noise Figure 4-1
4.3 Wideband Frequency Response 4-3
4.4 Maximum Input Power 4-4
4.5 Dynamic Range 4-4
5 Conclusion **5-1**

6 References 6-1
Appendix A RF Component Operating Frequency Ranges A-1
Appendix B Abbreviations and Acronyms B-1

List of Figures

Figure 1: Map of East Coast Sensor Deployments 1-3
Figure 2: Map of West Coast Sensor Deployments 1-4
Figure 3: Sensor RF Block Diagram 2-2
Figure 4: Cascaded gain and Noise Figure. 2-3
Figure 5: Swept Gain and Noise Figure 2-4
Figure 6: Bandpass Filter Frequency Response 2-6
Figure 7: Limiter Output Power vs. Input Power 2-7
Figure 8: LNA Gain from Manufacturer Datasheet with CBRS Band Shaded 2-8
Figure 9: LNA Noise Figure from Manufacturer Datasheet[6] with CBRS Band Shaded 2-8
Figure 10: Sample RSA FFT Analysis with 3605 MHz Input Signal 2-10
Figure 11. RSA Fundamental Signal and Spur Levels 2-11
Figure 12: RSA Displayed Average Noise Level and Noise Figure for Various Reference Level and Attenuator Settings 2-12
Figure 13: RSA Input Power Sweep with -25 dBm Reference Level 2-13
Figure 14: RSA Maximum Input Power for Various Reference Level and Attenuator Settings 2-14
Figure 15: RSA Dynamic Range for Various Reference Level and Attenuator Settings 2-15
Figure 16: Partitioning of Sensor RF Components into Preselector and SPU Assemblies 3-1
Figure 17: Preselector Block Diagram 3-4
Figure 18: Annotated photo of preselector assembly 3-6
Figure 19: Preselector Connector Panel 3-6
Figure 20: Preselector Mounted on Antenna Mast on Roof of Chesapeake Bay Bridge-Tunnel Island 4 Maintenance Building 3-7
Figure 21: Thermal Simulation of Preselector in Extreme Temperature 3-8
Figure 22: Internal Temperature Data for Deployed Preselectors, July-August 2025 3-9
Figure 23: SPU Block Diagram 3-10
Figure 24: SPU Power Management Block Diagram 3-11
Figure 25: SPU Control and Monitoring Block Diagram 3-12

Figure 26: Annotated Photo of SPU Assembly 3-15
Figure 27: SPU Connector Panel 3-16
Figure 28: SPU Mounted to Parapet on Roof of Chesapeake Bay Bridge-Tunnel Island 4 Maintenance Building 3-17
Figure 29: SPU Temperature Test with TEC Disabled 3-18
Figure 30: SPU High Temperature Test 3-19
Figure 31: SPU Low Temperature Test 3-20
Figure 32: Internal Temperature Data for Deployed SPUs, July-August 2025 3-21
Figure 33: Internal Temperature Data for GMM SPU, January 13-16, 2024 3-22
Figure 34: Full System Gain and Noise Figure 4-2
Figure 35: Full System Frequency Response 4-3
Figure 36: Full System Maximum Input Power 4-4
Figure 37: Full System Dynamic Range for Various Reference Level and Attenuator Settings 4-5

Figure A-1. Sensor RF Component Operating Frequency Ranges A-2

List of Tables

Table 1: Summary of CBRS SEA Sensor Deployments 1-2
Table 2. Summary of Bandpass Filter Measurements 2-6
Table 3: Additional Sensor Design Documents 3-2
Table 4: Preselector Component Part Numbers and Operating Temperature Ranges 3-5
Table 5: SPU Component Part Numbers and Operating Temperature Ranges 3-13
Table 6: SPU Temperature Control Setpoints 3-18
Table 7: Sensor Power Consumption 4-1

Table A-1. Sensor RF Component Operating Frequency Ranges A-1

1 Introduction

Citizens Broadband Radio Service (CBRS) is a radio frequency (RF) band in the United States spanning 3550 MHz to 3700 MHz, which is increasingly used for 4G long-term evolution (LTE) and 5G networks. Its applications include commercial services such as mobile and fixed wireless access networks, as well as private networks supporting operations at locations like corporate campuses and airports. Until recently, this portion of the RF spectrum was reserved exclusively for military systems - most notably a U.S. Navy radar system - and commercial satellite service ground stations. However, in 2020, the Federal Communications Commission (FCC) authorized use of the CBRS band by commercial and private entities alongside incumbent users, employing a new spectrum sharing methodology. This methodology, based on a multi-tiered and dynamic spectrum access model, is the first of its kind in large-scale wireless network deployment. While commercial and private use of the CBRS band has largely been 4G LTE and 5G networks to date, FCC rules do not limit use of the band to only those applications.

In 2021, the National Advanced Spectrum and Communications Test Network (NASCTN) was funded to perform a study to examine the effectiveness of this new spectrum sharing methodology. The study, entitled *CBRS Sharing Ecosystem Assessment (SEA)* [1], relies on a network of custom-designed spectrum monitoring sensors to collect data on the spectrum dynamics in locations where Navy incumbent systems may be present. NASCTN will publish the outcome of the overarching test campaign and resultant data. This report details the design of these sensors.

The CBRS SEA sensor design is the result of a highly collaborative effort between The MITRE Corporation and NASCTN. While MITRE served as the lead developer, many aspects of the design including RF architecture decisions and key component selections draw upon the collective experience of NASCTN team and lessons learned from previously deployed spectrum monitoring sensors. MITRE incorporated this input and applied its own expertise to evolve the design into a robust, field-ready system. In addition to design, MITRE's role included procurement, assembly, test, and deployment of the sensors.

The sensor was developed following an iterative approach. An initial prototype was built and deployed at several sites to evaluate the design's effectiveness, and to collect preliminary data for developing analysis capabilities. Due to time constraints some tradeoffs were made during prototype development, including constructing it so that part of the sensor had to be housed indoors and protected from the elements. Two prototype sensors were deployed in October 2022, in the vicinity of Naval Station Norfolk (Norfolk, VA): one on the roof of a high-rise building at Hampton University, and the other on the roof of a control tower at Norfolk International Terminal (operated by the Port of Virginia). After several months of operation at these sites, lessons learned from the prototypes were incorporated into plans for the production version of the sensor.

Although functionally similar to the prototype, the production version of sensor represented a significant redesign. The most notable improvement was repackaging the sensor into a sealed, weatherproof enclosure, enabling exclusively outdoor deployments. This change required a redesign of the sensor's power management to achieve a smaller form factor and the integration of temperature control. Additionally, the preselect filter was redesigned to protect the sensor from strong 5G emissions in the upper adjacent band—an issue identified during the prototype deployments (see Section 2.1.3 for details). Finally, the sensor was upgraded to support up to

two external antennas, whereas the prototype supported only one. Note that despite these physical differences, both versions of the sensor collect the same data.

At the time of this report's publication, ten sensors have been deployed of which nine remain operational. The first prototype sensor installed was replaced by a production sensor at that same site 16 months later. A summary of these sensor deployments is provided in Table 1. For further context, maps of the sensor locations on the East Coast and West Coast are shown in Figure 1 and Figure 2, respectively.

The following sections detail the design and implementation of the CBRS SEA sensor and present selected system measurement results. Accompanying this report is a documentation package that includes a complete set of schematics, parts lists and assembly drawings containing all of the information needed to reproduce the sensor. While the sensor was specifically designed to operate in the CBRS band, many of its RF components have wide operating frequency ranges and could be adapted to measure other bands. Appendix A presents a summary of the component frequency ranges and suggestions for adapting the sensor to other bands.

This report focuses on the sensor hardware; however, several other publications cover additional aspects of the sensor. For details regarding sensor calibration, refer to the National Institute of Standards and Technology (NIST) publication, "Noise Based Power Calibration Techniques for Mid-band Radio Frequency Sensors" [2]. For information on the sensor command and control and data acquisition software, refer to the National Telecommunications and Information Administration (NTIA) publication [3]. For further details on the data products produced by the sensors, refer to the NIST publication "Citizens Broadband Radio Service (CBRS) Sharing Ecosystem Assessment (SEA) Sensor Data Manual" [4].

Table 1: Summary of CBRS SEA Sensor Deployments

Deployment Date	Sensor Name	Location	Sensor Version
September, 2022	Green Mountain Mesa	Boulder, CO	Prototype[2]
October, 2022	Norfolk International Terminal	Norfolk, VA	Prototype[3]
October, 2022	Hampton University Tower	Hampton, VA	Prototype[3]
January, 2024	Green Mountain Mesa	Boulder, CO	Production
April, 2024	USMC Camp Pendleton	USMC Camp Pendleton, CA	Production
June, 2024	USS Midway Museum	San Diego, CA	Prototype[3]
July, 2024	US Coast Guard Tower Site, Mt Orizaba	Catalina Island, CA	Production
October, 2024	Naval Air Station Oceana	Virginia Beach, VA	Production
October, 2024	Island 4, Chesapeake Bay Bridge-Tunnel	Chesapeake Bay, VA	Production
July, 2025	Navy Building T17, Point Loma	San Diego, CA	Prototype[3, 4]

[2] Prototype sensor at Green Mountain Mesa was taken out of service when production sensor was installed in January 2024

[3] Preselect filter upgraded to same filter used in production sensor

[4] Sensor upgraded to support two antennas like production sensor

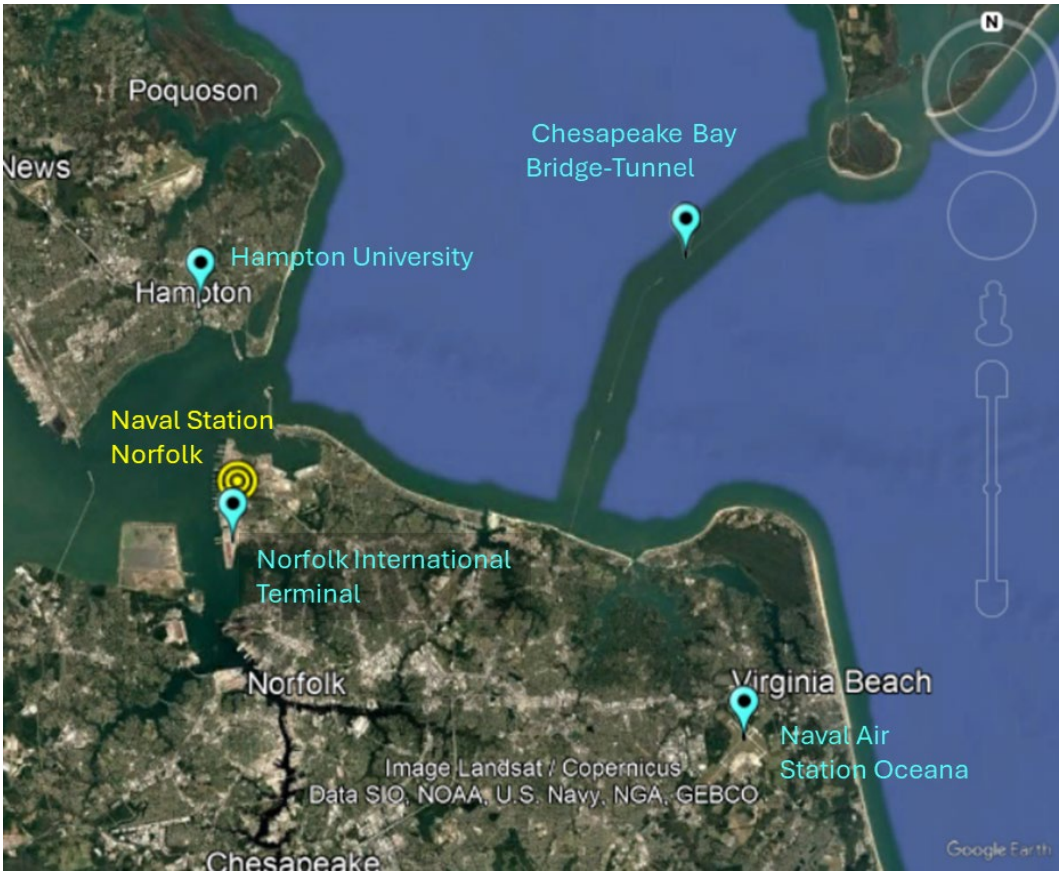

Figure 1: Map of East Coast Sensor Deployments

Figure 2: Map of West Coast Sensor Deployments

2 Sensor Overview

The CBRS SEA sensor was designed to analyze RF emissions in the 3550 to 3700 MHz CBRS band. It is a fully integrated, stand-alone, and calibrated system that captures the RF spectrum, computes power statistics and their distributions across time and frequency, and transfers these data products to a centralized repository for post-analysis.

The sensor was designed collaboratively by NASCTN and MITRE to operate over a multi-year measurement campaign, necessitating a highly reliable measurement system. NTIA's previous experience with long-term spectrum occupancy measurements [5] provided insights into typical reliability concerns and failure modes. In the NTIA multi-year study, the average reliability, or sensor uptime, was approximately 60.8%.

Building off NTIA's experience, the CBRS SEA sensor employed a modular design consisting of separate preselector and signal processing unit (SPU) assemblies, each housed in sealed, weatherproof enclosures as described in Section 3. The SPU included a thermoelectric cooler (TEC) unit with heating capability to regulate internal temperatures, allowing outdoor deployments in locations prone to hot or cold conditions. It also included a battery back-up to enable continued operation during short-term power outages.

The sensor used multi-stage low-noise amplifiers (LNAs) to maintain a low noise figure, along with configurable attenuation (integrated in its real-time spectrum analyzer, or RSA) to adjust for the unknown proximity of Citizens Broadband Radio Service Devices (CBSDs) at the various deployment sites. It also used a limiter to protect it from damage due to excessively strong signals. This architecture has allowed the sensor to measure emissions from CBSDs nearly 50 km away, while also surviving exposure to strong emissions from nearby incumbent radar systems.

These design features have resulted in high reliability. At the time of this report's publication, sensors have been deployed for a total of nearly 4000 sensor days, and they were operational more than 98% of that time.

The sensor also featured automated calibration using a calibrated noise source within the preselector. Periodic automated calibration allows the sensor to compensate for performance variations caused by temperature fluctuations and long-term aging over multiyear deployments, reducing measurement uncertainty.

The following sections provide additional design details for the production sensor.

2.1 RF System

Figure 3 shows the block diagram of the sensor's complete RF system. At the start of the RF signal path are the system inputs, which can be either of two antennas or a calibrated noise source. The antennas receive RF emissions in the CBRS band, while the noise source is used for periodic calibration. Typically, one antenna has an omnidirectional pattern and the other is directional, but any combination of antennas may be used. Two single pole double throw (SPDT) switches, referred to as Antenna Select Switch and Cal Select Switch, operate in tandem to route one of these three inputs to the remainder of the signal path.

Following the RF switches are an isolator and a bandpass filter. The filter rejects undesired emissions outside the CBRS band, while the isolator helps present a consistent impedance to the

filter input regardless of the RF switch state. This minimizes variation between the calibration path and antenna paths and reduces uncertainties in the calibration.

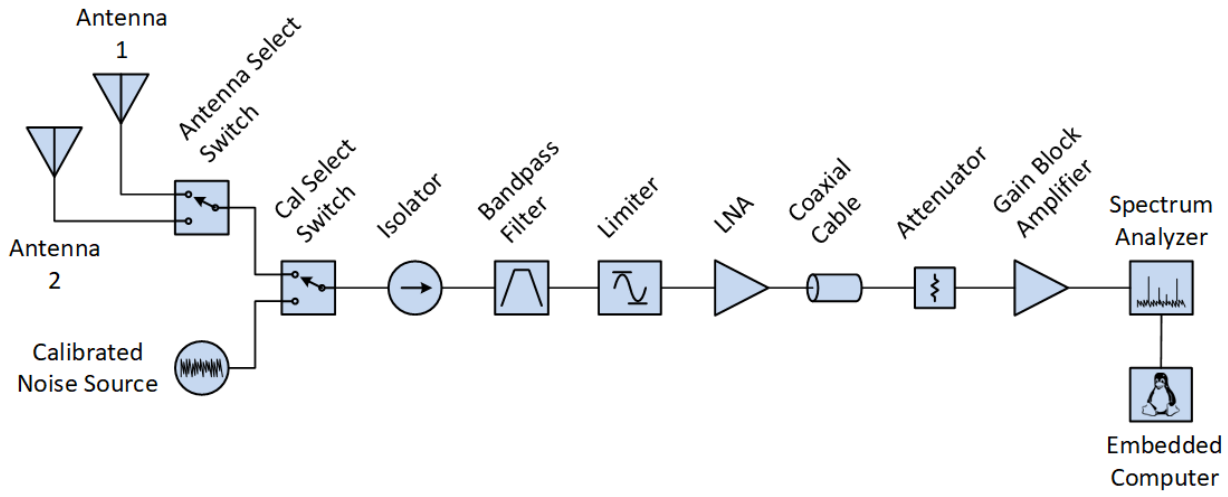

Figure 3: Sensor RF Block Diagram

Following the bandpass filter is an RF limiter that protects against excessively strong in-band emissions. Next is an LNA, which provides the gain needed to overcome system losses and minimize system noise figure. The LNA provides enough gain to tolerate up to 15 dB of subsequent losses before the next gain stage, with minimal degradation to the system noise figure. This enables the use of a long coaxial cable, if necessary, to physically separate groups of components and provide flexibility in sensor deployment. The components prior to and including the LNA should be positioned close to the antenna to minimize system noise figure, while the remaining components, which are typically larger and consume more power can be placed at a more convenient location farther away.

The attenuator following the coaxial cable compensates for cables of varying lengths. For each deployment, the attenuator value is selected so that the sum of the cable insertion loss and attenuator remains a constant. This ensures consistent RF performance across sensor sites, regardless of cable lengths due to unique installation requirements.

The final components in the RF signal path are the gain block amplifier and RSA. The gain block amplifier provides additional gain to minimize the noise figure contribution of the RSA and maintain a low overall system noise figure. The RSA, while capable of operating as a stand-alone fully featured test instrument, serves as the sensor's tunable RF digitizer. The RF signal at the RSA input is converted to a digital complex baseband signal with in-phase and quadrature (IQ) components. Subsequent processing on the IQ data is performed on the embedded computer.

The RF signal path was modeled in Keysight Genesys simulation software using measured parameters for all components. An RF cascade analysis was performed, and the resulting cascaded gain and noise figure are shown in Figure 4. This includes noise figure contributions from the RSA when configured in its typical deployment state[5]. The estimated gain from the sensor input to the RSA is approximately 32.5 dB, and the estimated noise figure is slightly less than 4 dB. This system model was a useful tool for determining the appropriate gain and

[5] RSA configuration: reference level = -25 dBm, input attenuator = 0 dB, preamp enabled. Measured noise figure = 24 dB.

attenuation at various stages of the signal path, helping to balance low noise figure with the ability to handle strong signals.

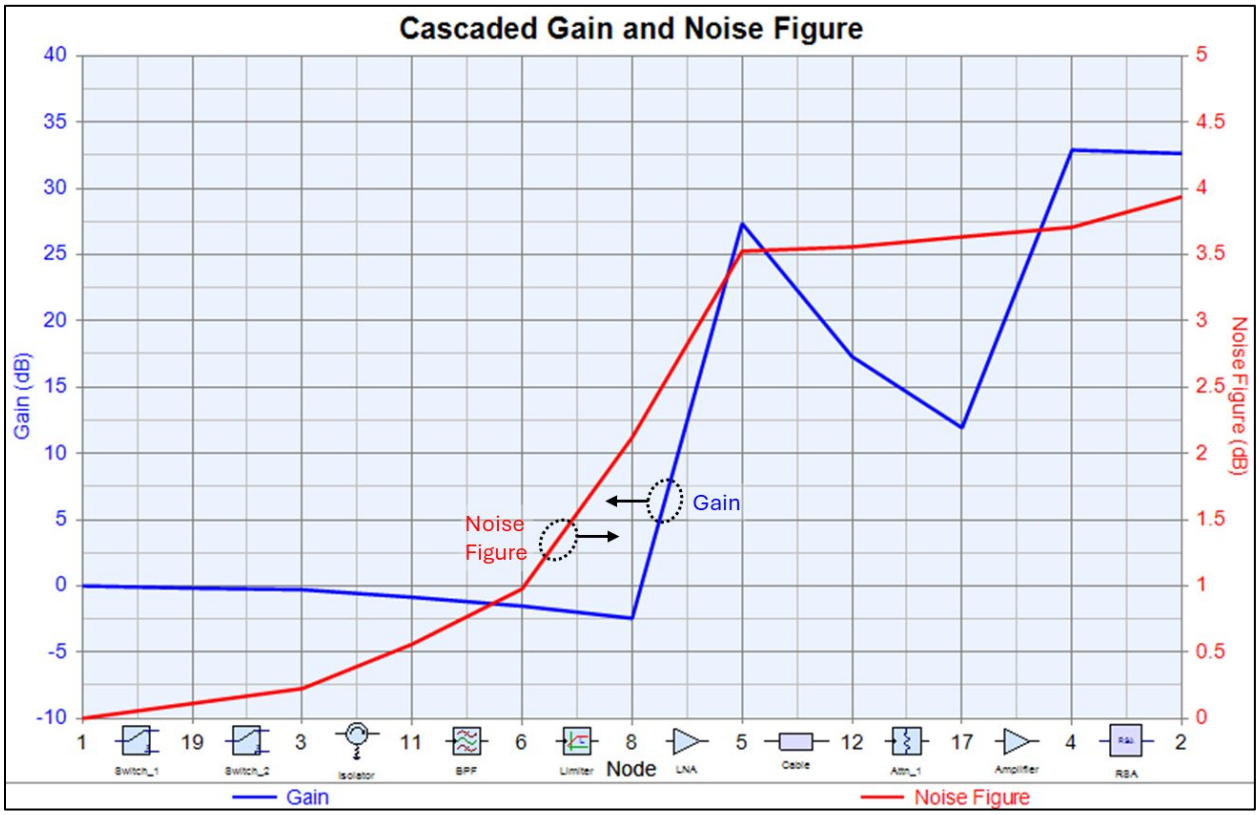

Figure 4: Cascaded gain and Noise Figure

A swept analysis was performed to examine gain and noise figure as functions of frequency, as shown in Figure 5. The results indicate a relatively flat gain of approximately 32–33 dB and a noise figure just under 4 dB across most of the CBRS band, up to approximately 3685 MHz. Beyond this frequency the insertion loss of the bandpass filter increases, resulting in reduced gain and higher noise figure. The filter was intentionally designed with this roll-off characteristic, and the rationale for this design choice is discussed in Section 2.1.3.

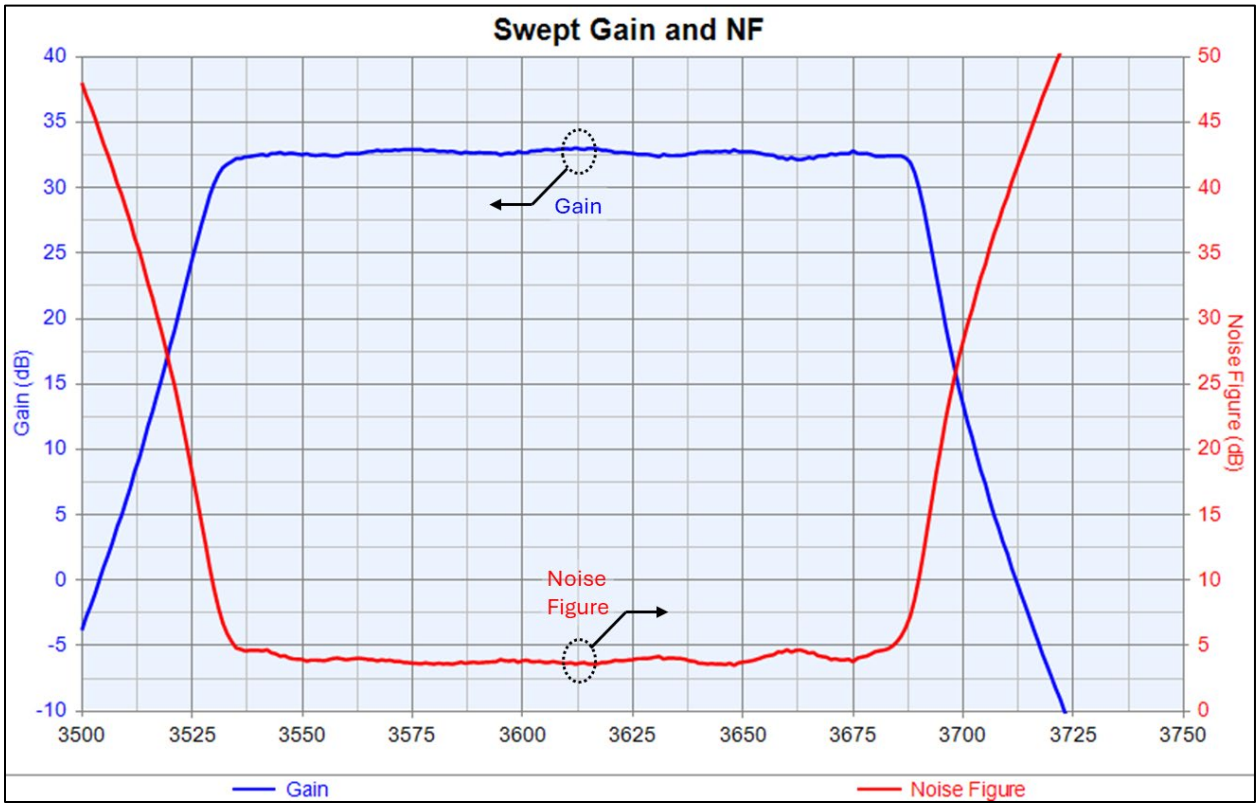

Figure 5: Swept Gain and Noise Figure

The following subsections provide further discussion of key components in the RF system. The complete sensor design is presented in Section 3.

2.1.1 Omnidirectional Antenna

A typical sensor deployment includes one omnidirectional antenna, the L-com HG3509U-PRO, to enable full 360° observation in the azimuth plane. This antenna has a specified frequency range of 3400 to 3700 MHz with 9 dBi gain. The antenna is omnidirectional in the azimuth plane, has a vertical 3 dB beamwidth of 11° and is vertically polarized. Since CBRS systems are terrestrial, the antenna's directive elevation pattern is advantageous as neighboring CBSDs will be predominately located within the 3° beamwidth of its elevation plane.

2.1.2 Directional Antenna

Many sensor deployments, though not all, include a directional antenna to increase gain in a region of interest and to allow for a comparison between omnidirectional and directional aggregate emissions from CBSDs. The directional antenna used is the KP-3DPFP20 from KP Performance Antennas which operates over a frequency range of 3500 to 3800 MHz. It has a specified 3 dB beamwidth of 15° in both the azimuth and elevation planes, a gain of 20 dBi, and is dual orthogonal polarized. While it is advertised as 45° slant polarized, the mounting orientation can also be configured for vertical/horizontal polarization although this may alter the pattern slightly. For SEA sensor deployments the antenna is typically oriented for

vertical/horizontal polarization, with the vertically polarized element connected to the sensor and the horizontally polarized element terminated with a 50 ohm load.

2.1.3 Bandpass Filter

The sensor uses a custom-designed cavity bandpass filter that maximizes measurement sensitivity within the CBRS band, while limiting desensitization from strong emissions in adjacent bands. The ideal theoretical filter for this application would exhibit very low insertion loss across the entire CBRS band and then begin to transition to high rejection just outside the band edges. However, data collected from deployed prototype sensors using filters with these characteristics showed vulnerability to strong adjacent band 5G emissions. C-band 5G begins at 3700 MHz, abutting the upper end of the CBRS band, and devices transmit at significantly higher power levels than those in the CBRS band. RSA measurements taken near the upper end of the CBRS band extends above 3700 MHz and overlaps the lower portion of C-band. The prototype sensor bandpass filter did not sufficiently attenuate these strong adjacent band 5G emissions beginning at 3700 MHz as analog filters require a transition region between their passband and stopbands causing the RSA to become saturated.

The production sensor filter design provided a greater rejection at the band edge to mitigate the impact of these adjacent band 5G emissions by reducing the filter's upper cutoff frequency to approximately 3690 MHz, creating a transition region that leads to more effective attenuation beginning at 3700 MHz. This change provided better protection against the strong adjacent band emissions, but at the expense of increased insertion loss and reduced measurement sensitivity at the upper end of the CBRS band.

The filter redesign also extended the passband slightly lower, to 3530 MHz, or 20 MHz below the lower edge of the CBRS band. This overlaps the upper end of the adjacent band, commonly referred to as the "3.45 GHz band", which spans 3450 to 3550 MHz. The CBRS band has an out-of-band emission requirement that is defined for the 20 MHz beyond its lower and upper band edges. This filter response enables the sensor to measure 20 MHz below the CBRS band (3530 to 3550 MHz) to gain insight into emissions levels within this transition region.

The new filter, Reactel part number 8C7-3610-X180S11, was measured with a network analyzer. The resulting frequency response is shown in Figure 6, and a summary of measured performance characteristics is provided in Table 2.

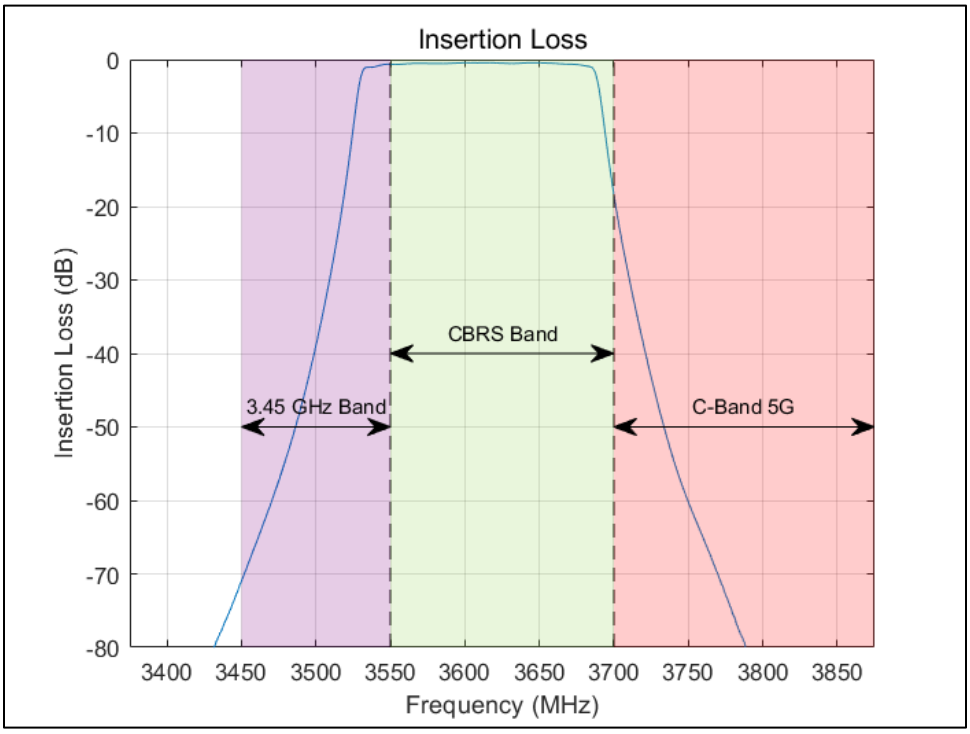

Figure 6: Bandpass Filter Frequency Response

Table 2. Summary of Bandpass Filter Measurements

Passband (3 dB cutoff)	3530 to 3690 MHz	
Insertion Loss at Center (3610 MHz)	-0.5 dB	
CBRS Band Flatness (excluding upper 20 MHz)	0.4 dB	
CBRS Band Upper Edge Insertion Loss (3700 MHz)	-18 dB	
>10 dB Rejection	<3524 MHz	> 3695 MHz
>30 dB Rejection	<3508 MHz	> 3712 MHz
>60 dB Rejection	< 3458 MHz	> 3752 MHz

2.1.4 Limiter

While the bandpass filter rejects strong out-of-band signals, strong *in-band* signals can still pose a risk of saturating or damaging the sensor's RF components. To protect against strong in-band signals, a Fairview Microwave FMLM2003 limiter is placed before the LNA, the first active component in the signal path and one that is susceptible to damage from excessively strong signals.

The limiter's maximum output power, known as "leakage", is specified as +13 dBm with a +30 dBm continuous-wave (CW) input across the frequency range 20 MHz to 4000 MHz. However, measurements at CBRS frequencies with input power up to +20 dBm (Figure 7), indicate a leakage of approximately +9 dBm. Although the output could still exceed +9 dBm for inputs above +20 dBm, the SEA sensor is not expected to be deployed at sites where it would be exposed to such conditions.

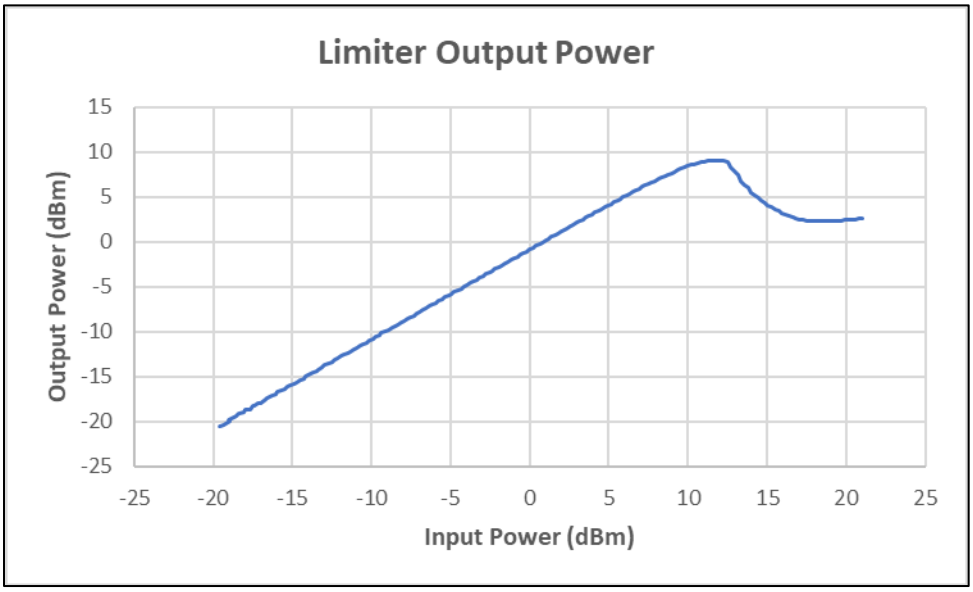

Figure 7: Limiter Output Power vs. Input Power

A cascade analysis demonstrated that with a maximum limiter output power of +9 dBm and a combined insertion loss of 15 dB for the coaxial cable and attenuator shown in Figure 3, the damage level of the active components downstream in the RF signal path – namely the LNA, gain block amplifier and RSA - will not be exceeded.

The limiter enables the sensor to operate with maximum sensitivity in the vicinity of an incumbent radar system, as long as the sensor is not in the main lobe of the radar antenna. Any radar with a rotating antenna will periodically be directed towards the sensor, and may momentarily saturate but not damage the sensor. As the radar antenna rotates out of the sensor's main lobe, the sensor will continue to operate at maximum sensitivity.

The deployed sensors at sites such as Point Loma and Norfolk International Terminal demonstrate the robustness of this design. These sensors, which are in close proximity to Naval Base San Diego and Naval Station Norfolk, respectively, have performed reliably despite frequent exposure to strong emissions from an incumbent rotating antenna radar.

2.1.5 Low Noise Amplifier

The LNA used in the sensor is the LiConn LNA02004000A. This wideband LNA operates from 200 MHz to 4.0 GHz. As the first gain stage in the RF signal path, the LNA's gain and noise figure significantly impact the overall system noise figure. In the CBRS band, the LNA's typical gain is 29 dB (Figure 8) and its typical noise figure is 1.3 dB (Figure 9). The LNA is rated for an operating temperature range of -45° C to +85° C, which enables usage in non-temperature-controlled environments such as those where the sensor may operate.

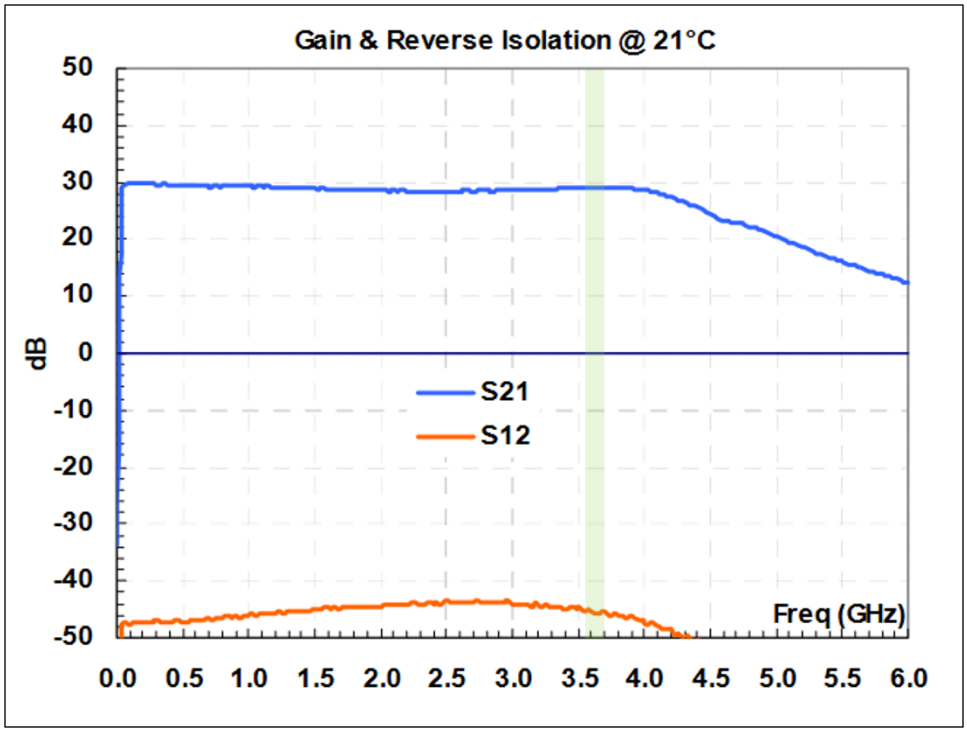

Figure 8: LNA Gain from Manufacturer Datasheet[6] with CBRS Band Shaded

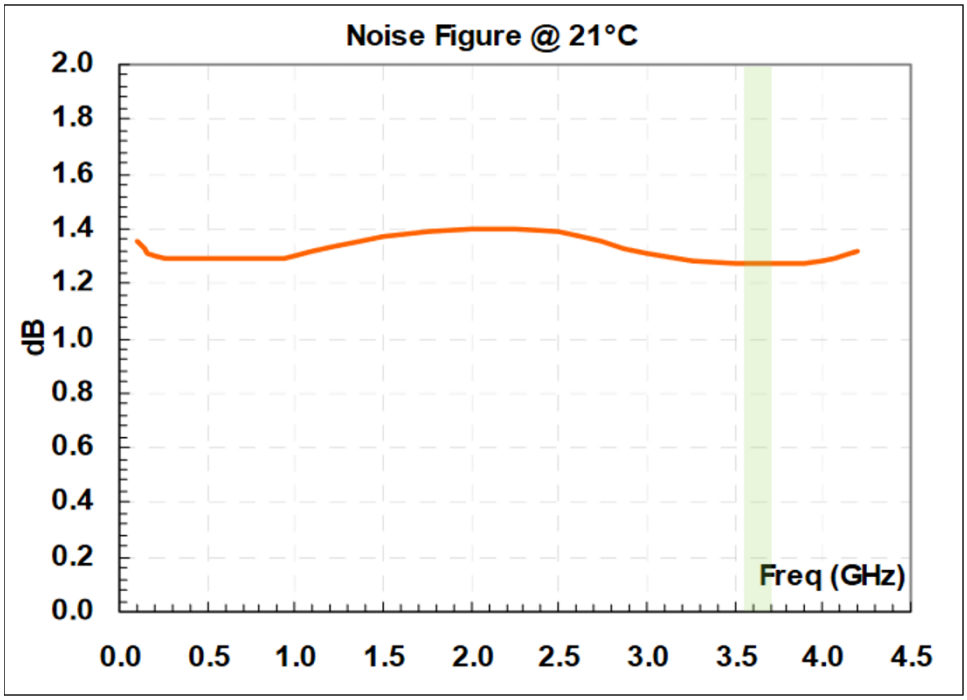

Figure 9: LNA Noise Figure from Manufacturer Datasheet[6] with CBRS Band Shaded

[6] LiConn, "LNA02004000A, 0.2 GHz ~ 4.0 GHz Wide Band Low Noise Amplifier," [Online]. Available: https://www.liconn.com/products/LNA02004000A.pdf. [Accessed 19 11 2025]

2.1.6 Gain Block Amplifier

The gain block amplifier used is a Mini-Circuits ZX60-83LN-S+, a wideband amplifier with a specified operating frequency range of 500 MHz to 8.0 GHz. Although Mini-Circuits markets this device as an LNA it is referred to as a gain block in this design because it serves as a second-stage amplifier, primarily intended to increase the gain at a specific point in the signal path. The amplifier provides a typical gain of 21 dB in the CBRS band and has an output 1 dB compression point (P1dB) of nearly 20 dBm. P1dB is a key consideration for amplifiers, especially in later stages, to ensure it does not limit the cascaded compression point of the overall system. The amplifier is rated for an operating temperature range of -40° C to +85° C.

2.1.7 Real-Time Spectrum Analyzer

A market survey was conducted to identify RSAs, spectrum-monitoring receivers, and software-defined radios tunable over the CBRS band, capable of acquiring at least 20 MHz instantaneous bandwidth and transferring digital baseband IQ data over a universal serial bus (USB) or Ethernet interface. A number of candidates were identified and evaluated for RF performance, power consumption, size, operating temperature range and cost. Several underwent laboratory testing to further assess RF performance, and the Tektronix RSA507A was ultimately selected.

The RSA507A real-time spectrum analyzer (RSA) tunes from 9 kHz to 7.5 GHz and provides up to 40 MHz instantaneous bandwidth. It uses a USB 3.0 interface to transfer IQ data to a host computer in IQ acquisition mode. It draws 15 W, operates from -10°C to +55°C, and is housed in a rugged 30.0 cm x 27.2 cm x 6.9 cm enclosure.

Since the RSA507A specifications cover a broad frequency range, laboratory measurements were performed to examine several key RF performance characteristics specifically within the 3550 to 3700 MHz CBRS band. First amplitude and spur levels were measured while sweeping an input signal across the RSA's 40 MHz maximum instantaneous bandwidth. The RSA was configured with a 3600 MHz center frequency, -40 dBm reference level, and 40 MHz bandwidth. A signal generator produced a -40 dBm CW input that was swept in 1 MHz steps across the analyzer's frequency range. At each step, IQ data was acquired from the RSA, and a fast Fourier transform (FFT) analysis was performed to determine the fundamental signal and spur levels.

Figure 10 illustrates an FFT of IQ data at an input frequency of 3605 MHz. The green marker indicates the input signal; the red markers indicate the three strongest spurs. Note that for an instantaneous bandwidth of 40 MHz, the RSA operates with an IQ sample rate of 56 Msps, which results in a full FFT bandwidth 56 MHz. This oversampling and the resulting excess bandwidth are intentional and necessary to prevent aliasing. However, the outer edges of that bandwidth are shaped by the RSA's anti-aliasing filters so only the central 40 MHz should be used. To emphasize this, frequencies outside the 40 MHz usable bandwidth are shaded orange in Figure 10.

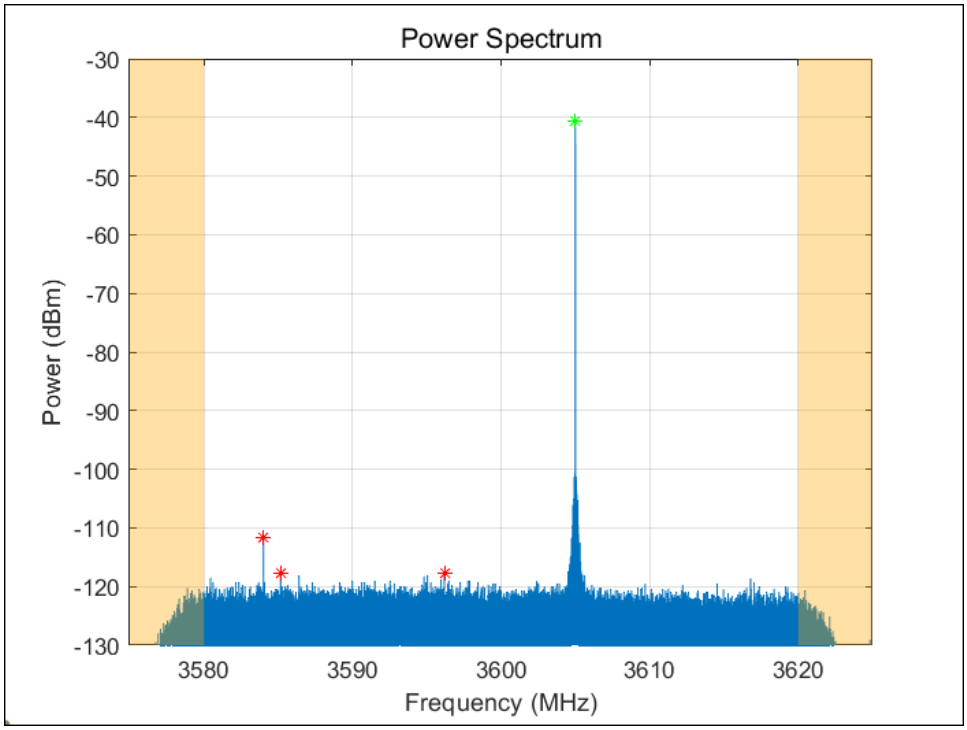

Figure 10: Sample RSA FFT Analysis with 3605 MHz Input Signal

An FFT analysis, similar to Figure 10, was performed at each step of the frequency sweep. Figure 11 shows the resulting fundamental signal level and the relative spur levels. The upper subplot displays the fundamental level, which varies approximately 0.2 dB across the 40 MHz band, and the lower subplot displays the relative spur levels. The largest spur level never exceeded 71 dB below the fundamental for any input frequency within the 40 MHz band, and in many cases the 2nd and 3rd spurs were indistinguishable from the noise.

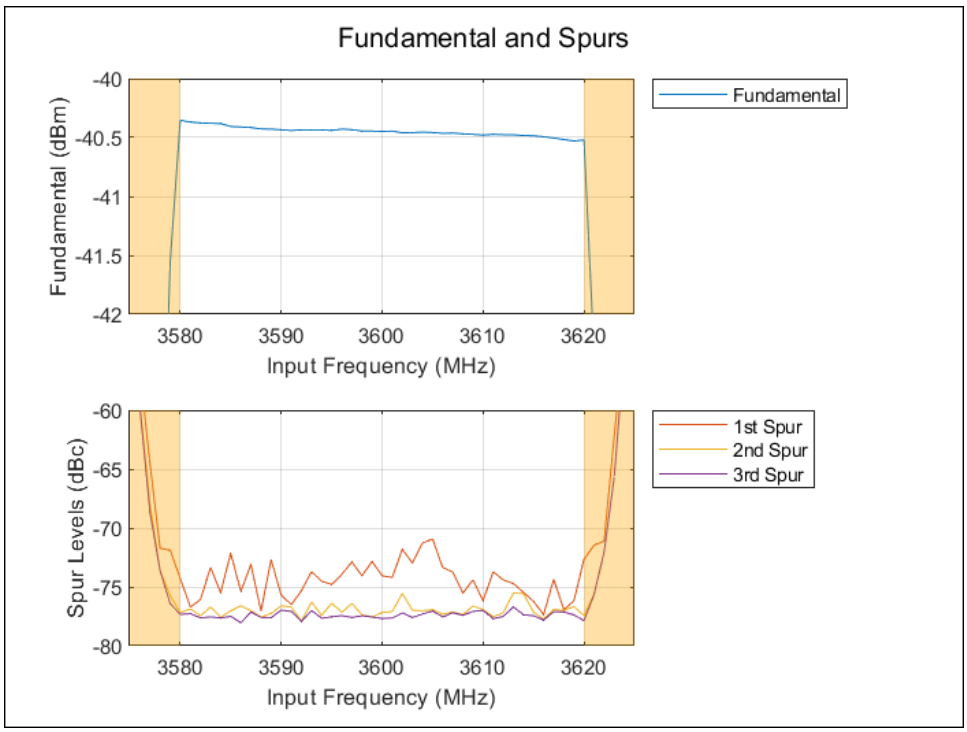

Figure 11. RSA Fundamental Signal and Spur Levels

Next, the displayed average noise level (DANL) was measured to characterize the RSA noise performance. For these measurements, the RSA was configured for a center frequency of 3625 MHz and sample rate of 56 Msps. Since DANL is dependent on the RSA amplitude settings, the measurement included a range of RSA reference levels and internal attenuator values – instrument settings that are independently configurable. Whenever possible the attenuator was set to a fixed offset of 25 dB greater than reference level (for example, a reference level of -25 dBm with an attenuator of 0 dB, a reference level of -20 dBm and with an attenuator of 5 dB, etc.). For reference levels less than -25 dBm, this was not possible since the attenuator has a minimum value of 0 dB.

The RSA RF input was terminated with a 50-ohm load when performing these measurements. IQ data from each measurement and used to compute the DANL. and shown in Figure 12. Blue points indicate where the 25 dB attenuator offset was possible; orange points indicate where the attenuator was fixed at 0 dB. This figure shows a minimum DANL of approximately -155 dBm/Hz measured with the lower reference-level settings, which falls within the range specified in the RSA datasheet. The equivalent noise figure is shown on the right axis of Figure 12. Although relatively high, this range of noise figures is typical of signal analyzers and with proper design of the RF signal path, a low overall noise figure can still be achieved as shown in the cascaded noise figure analysis in Figure 4.

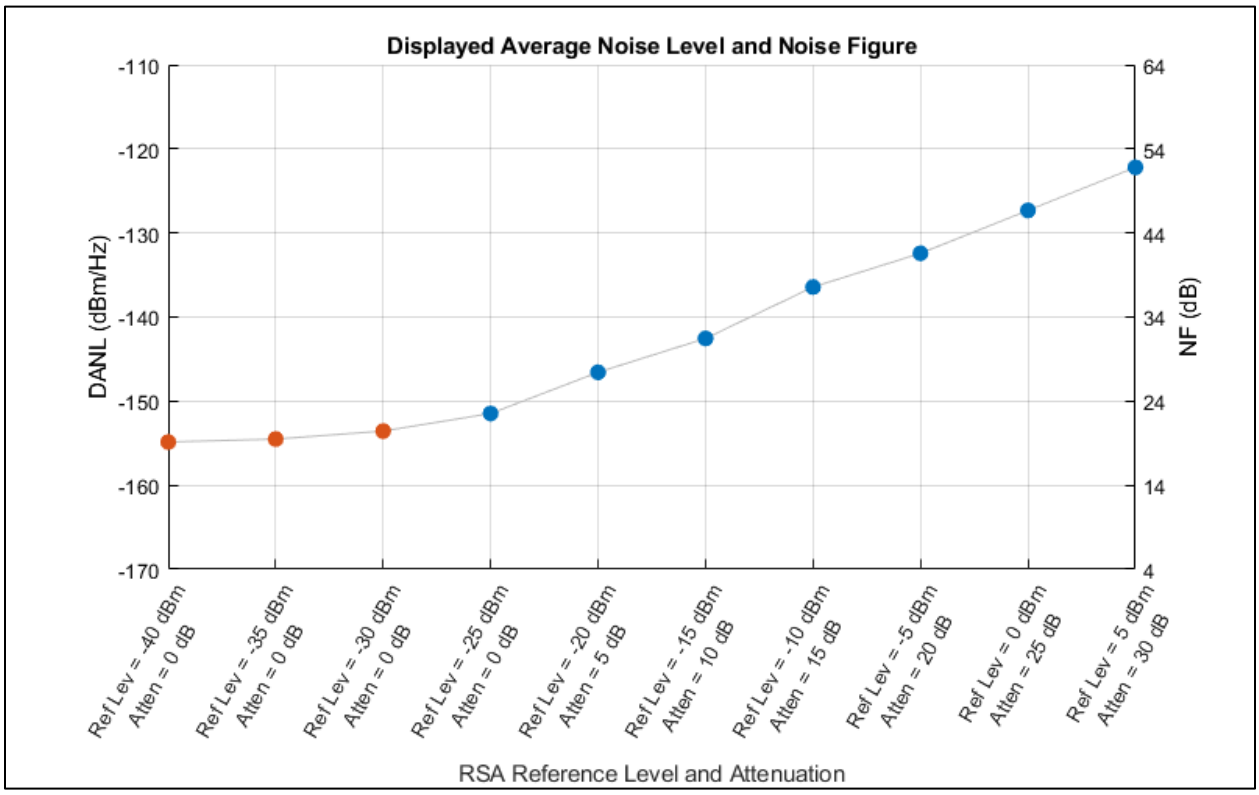

Figure 12: RSA Displayed Average Noise Level and Noise Figure for Various Reference Level and Attenuator Settings

Finally, to characterize the strong signal performance of the RSA, the maximum input power was measured. For these measurements the RSA was configured with the same center frequency (3625 MHz) and sample rate (56 Msps) as was used for the DANL measurements. Also similar to the DANL measurements, the RSA maximum input power is dependent on the RSA amplitude settings, so the measurement was performed with the same range of reference level and attenuator settings.

For each measurement, an RF signal generator produced a 3625 MHz CW signal at increasing power levels. At each input power level, IQ data was acquired and FFT analysis was performed to determine the measured power. The measurements were plotted, and the maximum input power was determined by observing how the measured signal level varied with increasing input levels.

An example plot, with the RSA reference level set to -25 dBm and attenuator set to 0 dB. is shown in Figure 13. The points in this plot show the RSA-measured power for a range of input power levels. The color of the points represents the RSA acquisition status; blue points indicate no acquisition anomaly while red points indicate that an analog-to-digital converter (ADC) overrange condition occurred. The gray line in the background is a trendline representing the ideal case, where the measured power equals the input power with no limitations.

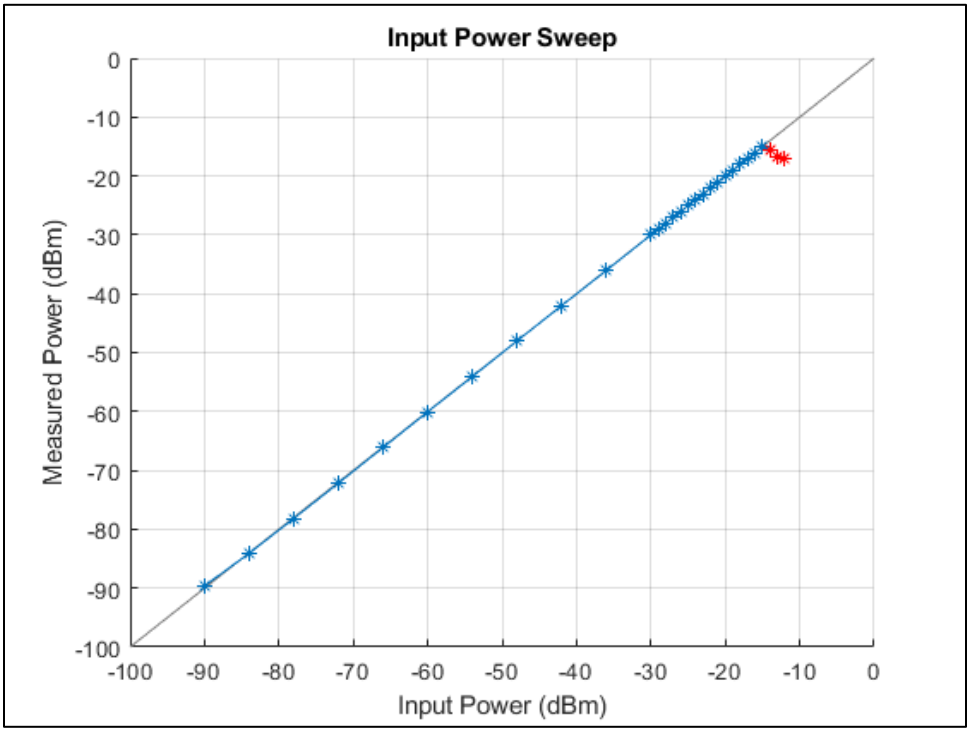

Figure 13: RSA Input Power Sweep with -25 dBm Reference Level

For all blue points, where an ADC overrange condition *does not* occur, the measured signal level closely matches the trendline, indicating that gain compression is not present. As the input level increases, a threshold is reached at which the RSA reports an ADC overrange condition (red points). When this occurs, large distortion products in the power spectrum draw power away from the fundamental, resulting in an abrupt reduction in the fundamental level even though the input level continues to rise.

Conventional RF components such as amplifiers generally exhibit a more gradual transition into compression. The output power versus input power curve initially deviates from the trendline by a small amount, with this deviation progressively increasing as the input power continues to rise. While the RSA does include these convention components in its signal path, it is designed so that the ADC input range is generally exceeded well before the rest of the signal path exhibits significant compression. Thus, the abrupt reduction in the measured fundamental level is due to the ADC overrange condition rather than a gradual compression from amplifiers and other components. Because of this characteristic, the maximum input power is simply defined as the highest input power that *does not* cause an ADC overrange condition.

The resulting maximum input power for a range of reference levels and attenuator settings is shown in Figure 14. As with the DANL plot in Figure 12, blue points indicate measurements with a 25dB RSA attenuator offset from the reference level, while orange points indicate measurements where the attenuator was fixed at 0 dB. This plot demonstrates how the RSA maximum input power increases with increasing reference level and attenuator value.

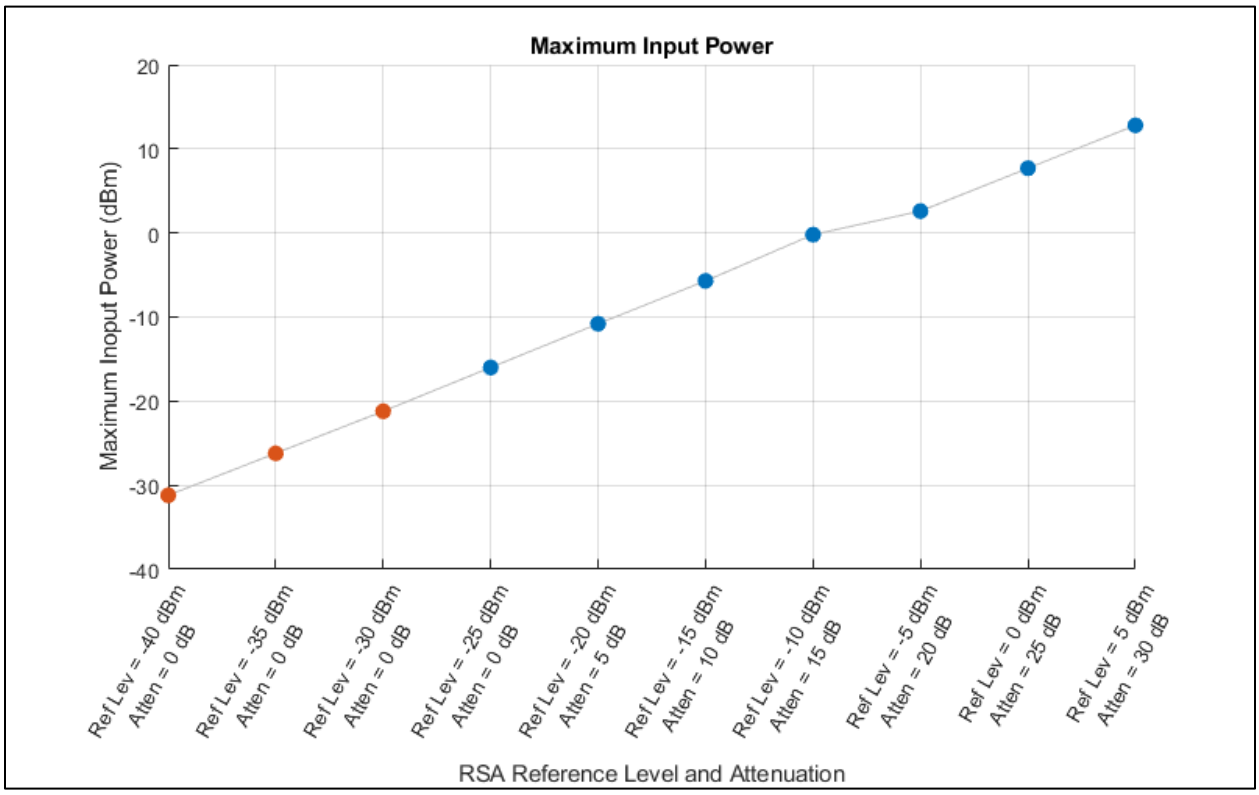

Figure 14: RSA Maximum Input Power for Various Reference Level and Attenuator Settings

These noise and maximum input power results provide an indication of the range of signal levels that the RSA can measure, otherwise known as dynamic range. There is no single industry standard definition for dynamic range, it's defined based on application. For the SEA sensor, dynamic range is defined as the difference between the maximum input power that does not cause an ADC overrange condition and the noise power within a 10 MHz measurement channel.

Figure 15 combines the noise and maximum input power measurements to illustrate the RSA dynamic range. Each vertical line in the figure depicts the dynamic range for a single combination of reference level and attenuator settings. The bottom of the line represents the equivalent noise power in a 10 MHz channel, derived from the measured DANL, which is an indication of the RSA measurement sensitivity. The top of each line represents the maximum CW input signal level that does not causing an ADC overrange condition. The dynamic range is the difference between these values.

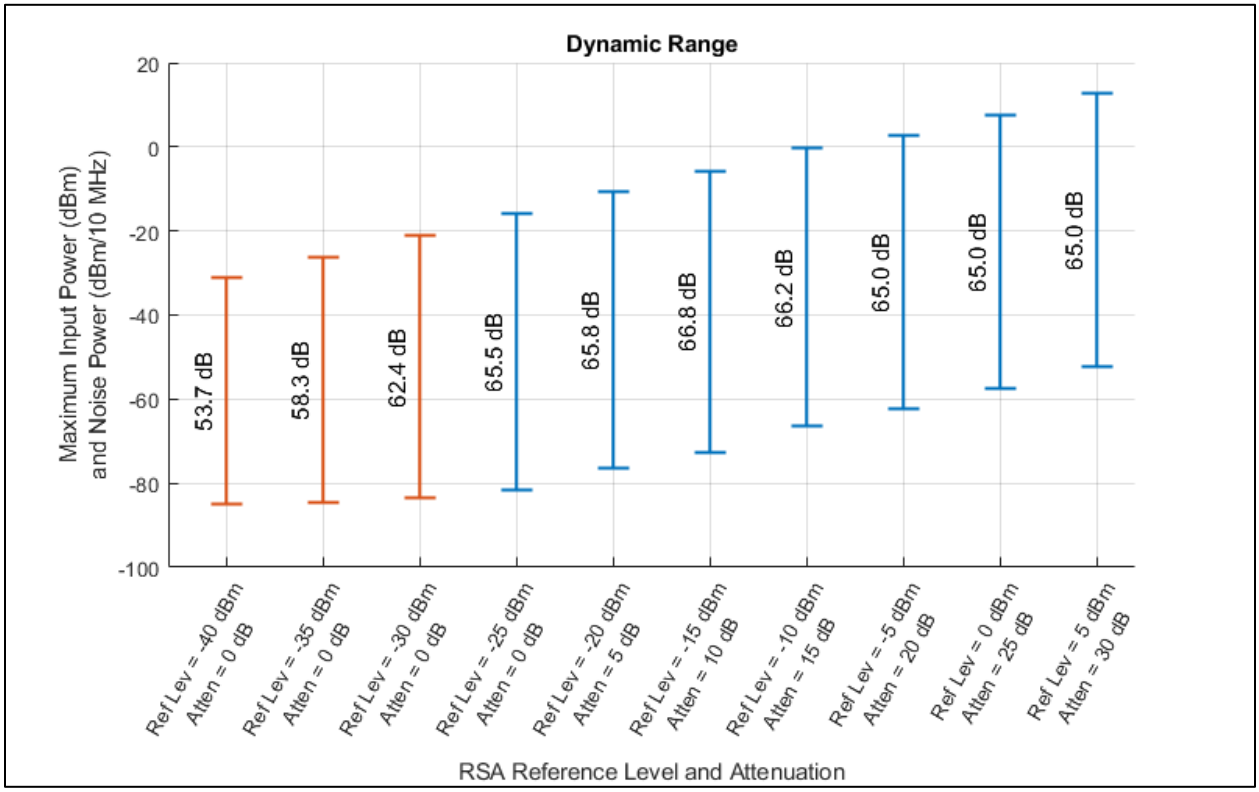

Figure 15: RSA Dynamic Range for Various Reference Level and Attenuator Settings

Figure 15 highlights the RSA's ability to accommodate various ranges of input signal levels and demonstrates that the reference level and attenuator can be reduced to maximize sensitivity, but below a certain point the sensitivity improvement is negligible while the dynamic range impact is significant. These dynamic range measurements were performed with a fixed offset of 25 dB between RSA reference level and attenuator value, whenever possible. This offset was determined through additional testing, not presented in this report, to achieve an optimal balance of dynamic range and sensitivity. Increasing the offset, to an extent, improves dynamic range at the expense of DANL. However, for offsets greater than 25 dB, the dynamic range improvement is negligible while the impact on DANL is significant. Conversely, offsets less than 25 dB yielded only small improvements in DANL but with significant impact to dynamic range.

2.1.8 Embedded Computer

Edge processing of the IQ data is performed on a SimplyNUC NUC13TZi7 small form factor computer, which features a 13th Gen Intel® Core™ i7 processor, 32 GB RAM, and 1 TB local M.2 storage, running the Ubuntu operating system. This computer was selected for its small size and powerful computing capabilities, enabling real-time processing of IQ data. It also includes a USB 3.2 interface to support the high-speed transfer of IQ data from the RSA.

Because computer technology evolves rapidly, smaller, more powerful and more energy-efficient computers should be considered for future sensor variants.

3 Sensor Implementation

The sensor has been designed and implemented to optimize performance while ensuring flexibility and ease of deployment. Certain RF components should ideally be located near the antennas to minimize system noise figure, while others may benefit from placement in less constrained areas due to their larger size, weight and power consumption. To accommodate various field installation requirements, the system was partitioned into two main assemblies: the preselector and the SPU.

As shown in Figure 16, the RF components from the antenna select switch to the LNA are housed in the preselector, while the attenuator, amplifier, RSA and embedded computer are housed in the SPU. Additional support components for functions such as power management, communication and control are not shown in this RF system diagram; further design details on these assemblies are presented in the following sections.

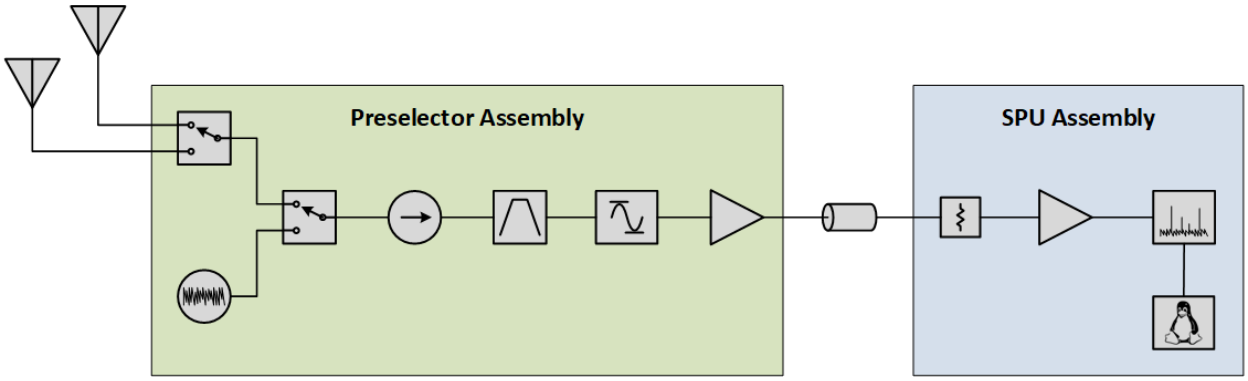

Figure 16: Partitioning of Sensor RF Components into Preselector and SPU Assemblies

The components in the preselector are all relatively small, draw little power, and can tolerate an operating temperature range of at least 50° C. To facilitate installing these components close to the antennas, which is necessary to minimize antenna cable lengths and, therefore, minimize system noise figure, the preselector is assembled into a small, weatherproof enclosure that can be mounted on a mast directly below the antenna. Since the preselector components draw little power and generate minimal internal heat, the enclosure was designed without integrated temperature control, with the expectation that internal temperatures will rarely, if ever, exceed the operating limits.

In contrast, the SPU assembly contains components that are larger, heavier and dissipate more power. These components can be located farther from the antenna without sacrificing system performance. Like the preselector, the SPU is assembled into a weatherproof enclosure to enable deployment in areas exposed to the elements. However, due to the heat generated by the internal components (particularly the embedded computer and RSA) and the lack of air circulation in the sealed enclosure, TEC was included to prevent internal temperatures from exceeding operating limits. The TEC unit also has heating capability to prevent the internal temperature from falling below the operating range, although this feature is unlikely to be needed in the climates where the sensor is intended to be deployed.

The system can tolerate up to 15 dB of coaxial cable loss between the preselector and SPU. This allows for up to 40 meters of low-loss coaxial cable to be used between assemblies, providing

flexibility in component installation to accommodate deployment sites with varying requirements.

3.1 Detailed Design Documentation

A complete set of schematics, parts lists and assembly drawings have been created, containing all the details needed to reproduce the sensor. These documents are provided as set of Portable Document Format (PDF) files external to this report. Send requests for these documents to NASCTN@nist.gov. Table 3 provides a summary of these documents.

The design documents are organized into a two-tier hierarchical structure. At the top tier are the system-level documents; the system electrical diagram, system cable assembly drawings, and system parts list. These documents present the preselector and SPU as abstract blocks and incorporate other system-level components, including antennas and interconnect cables. At the second tier are document sets for the preselector and SPU, each consisting of an electrical diagram, assembly drawing, cable assembly drawing and parts list.

Please note that the references to companies and products in this document and the accompanying design documents do not constitute an endorsement or recommendation by The MITRE Corporation, nor do they imply that the identified products are the only or best options available. Furthermore, while reasonable efforts have been made to ensure the accuracy of the design documentation, MITRE makes no warranties regarding the completeness or reliability of the information provided.

Table 3: Additional Sensor Design Documents

System Level Documents	Preselector Documents	SPU Documents
System Electrical Schematic	Preselector Electrical Schematic	SPU Electrical Schematic
System Cable Assembly Drawings	Preselector Assembly Drawings	SPU Assembly Drawings
System Parts List	Preselector Cable Assembly Drawings	SPU Cable Assembly Drawings
	Preselector Parts List	SPU Parts List

The following sections describe key aspects of the design of the preselector and SPU. However, they present the design at the block diagram level and do not include all details. For complete details, refer to the external design documents.

3.2 Preselector Assembly

A block diagram of the preselector assembly is shown in Figure 17 and part numbers for key components are provided in Table 4. The preselector contains the RF system components from the antenna select switch to the LNA. These components are partitioned into a separate assembly to facilitate installation close to the antenna.

In addition to the RF components, the preselector includes several supporting control, power management, and environmental monitoring components. A key feature of the design is the network-enabled controller, which enables remote management of the preselector's operating states via Ethernet. The controller has four integrated relays with a shared common terminal, used to distribute 28 V_{DC} to various components. Two of these relays set the control voltages for

the two coaxial switches: the antenna select switch and the calibration select switch. When the sensor is conducting measurements, the switches are set in tandem so that one of the two external antenna inputs is selected as the system input. During periodic calibrations, the calibration select switch is set to select the noise source as the system input. Also during calibration, a third relay in the controller enables the noise source by providing a 28 V_{DC} supply voltage. The noise source is typically disabled except when the sensor is performing a calibration. Finally, a fourth relay in the controller presents a 28 V_{DC} supply voltage to a 5V DC-DC converter, which in turn supplies 5 V_{DC} to the LNA. Although the controller has the ability to disable the LNA, it typically remains enabled during normal operation.

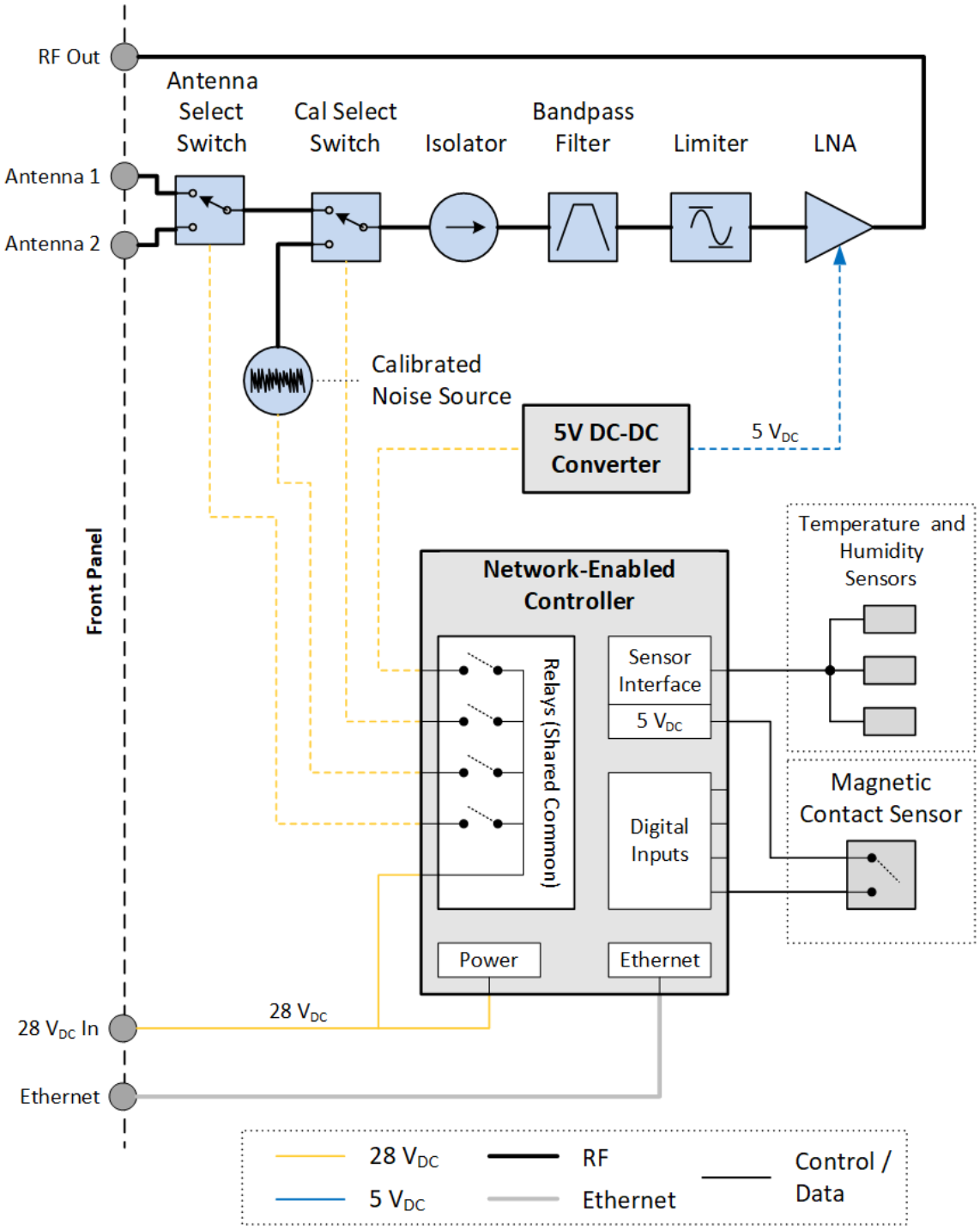

Figure 17: Preselector Block Diagram

The controller also includes a digital sensor interface that can communicate with multiple external sensors. The preselector assembly contains three sensors that report temperature and humidity through this interface. One of these is a combined temperature and humidity sensor, centrally located within the assembly. The other two are temperature sensors attached to the metal packages of the LNA and noise source to measure device temperatures. Monitoring these

parameters is necessary for sensor calibration, as well as for verifying the functionality and integrity of the sensor system and supporting the credibility of its RF measurements.

Finally, a digital input on the controller monitors the state of a magnetic contact sensor placed on the enclosure door indicating whether the door is open or closed. This feature can be used to detect tampering the preselector, which is important given that the sensor is intended to be deployed in remote locations and not under the physical control of the operators.

Table 4: Preselector Component Part Numbers and Operating Temperature Ranges

Component	Manufacturer	Part Number	Temperature Range
Antenna select switch Cal select switch	Dow-Key	401-6308	-25 to +65°C
Isolator	CentricRF	CI2040	-40 to +70°C
Bandpass filter	Reactel	8C7-3610-X180S11	-40 to +85°C
Limiter	Fairview Microwave	FMLM2003	0 to +50°C
LNA	LiConn	LNA02004000A	-40 to +85°C
Noise source	Keysight	346B	0 to +55°C
Network-enabled Controller	ControlByWeb	X410-I	-40 to +80°C
DC-DC converter	Acopian	28EB5E250	-20 to +70°C

The preselector is assembled into a 36 cm x 31 cm x 18 cm fiberglass-reinforced polycarbonate weatherproof enclosure with a National Electrical Manufacturers Association (NEMA) 4X / IP66 rating. This enclosure was selected to protect the internal electronics from the environmental conditions expected in locations where the sensor is intended to be deployed, including precipitation, solar radiation, and corrosive sea spray. All components are mounted on an aluminum base plate and interconnected with various coaxial, power, and control cables. A photo of the internal assembly, with components annotated, is shown in Figure 18.

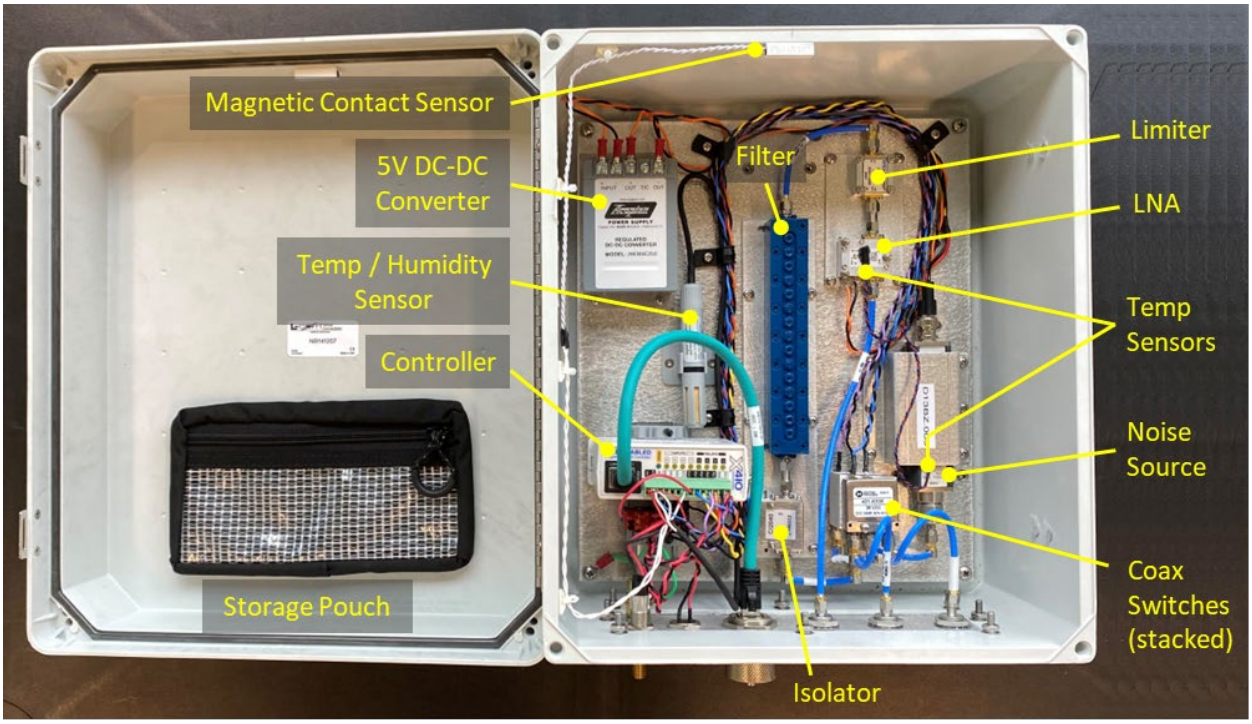

Figure 18: Annotated photo of preselector assembly

The bottom side of the enclosure is modified with a connector panel, shown in Figure 19, featuring feed-through connectors for the two antenna inputs, the RF output, a 28 V_{DC} supply voltage and Ethernet.

Figure 19: Preselector Connector Panel

Finally, Figure 20 shows a photo of a preselector deployed at the Chesapeake Bay Bridge-Tunnel (CBBT) sensor site in October 2024. The mast is secured to the parapet on the roof of the Island 4 maintenance building, with the preselector mounted just below the antennas to minimize the antenna cable lengths. A longer set of cables, including a coaxial cable, DC power cable, and

Ethernet cable, runs down from the preselector and exits the frame to the right, leading to the SPU which is out of view (refer to Figure 26).

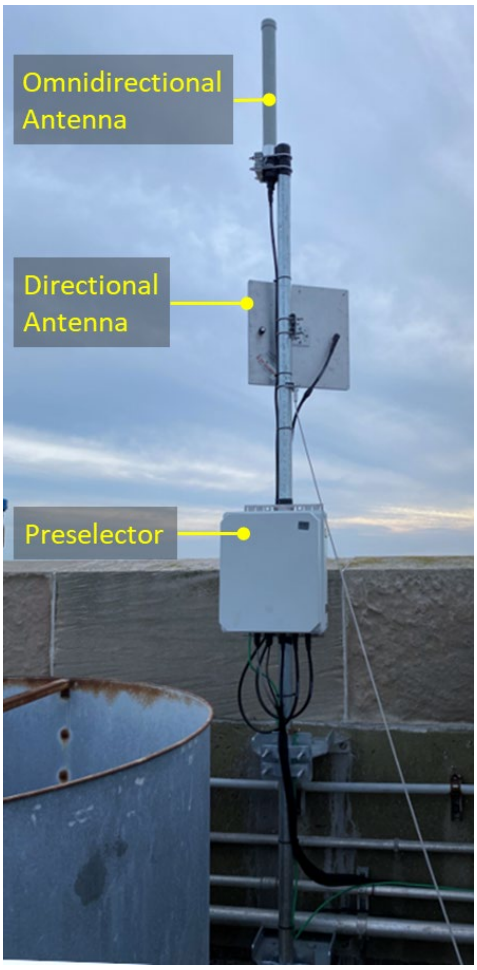

Figure 20: Preselector Mounted on Antenna Mast on Roof of Chesapeake Bay Bridge-Tunnel Island 4 Maintenance Building

3.2.1 Preselector Thermal Testing

Although the preselector components do not consume significant power and therefore generate little heat, they are sealed inside a waterproof, airtight enclosure with no active cooling. As such, a thermal analysis was performed to predict the air temperatures inside the enclosure under extreme conditions. The preselector was modeled in Ansys Icepak simulation software, and a thermal simulation was run. The simulation used an ambient temperature of 43.3° C, which is the maximum expected temperature[7] specified in MIL-HDBK-310 [6] even though it's unlikely to be reached in locations where the sensor is intended to be deployed. Additionally, it assumed maximum exposure to solar radiation and the maximum preselector power consumption of 5.6 W. The results are shown in Figure 21. Under these conditions, the simulation predicted that the temperature inside the enclosure would reach nearly 51.9° C, or 8.6° C above ambient.

[7] MIL-HDBK-310 section 5.2. Ambient temperature used in analysis is the one-percent hot temperature for "basic regional type," which is the regional type that covers the continental United States.

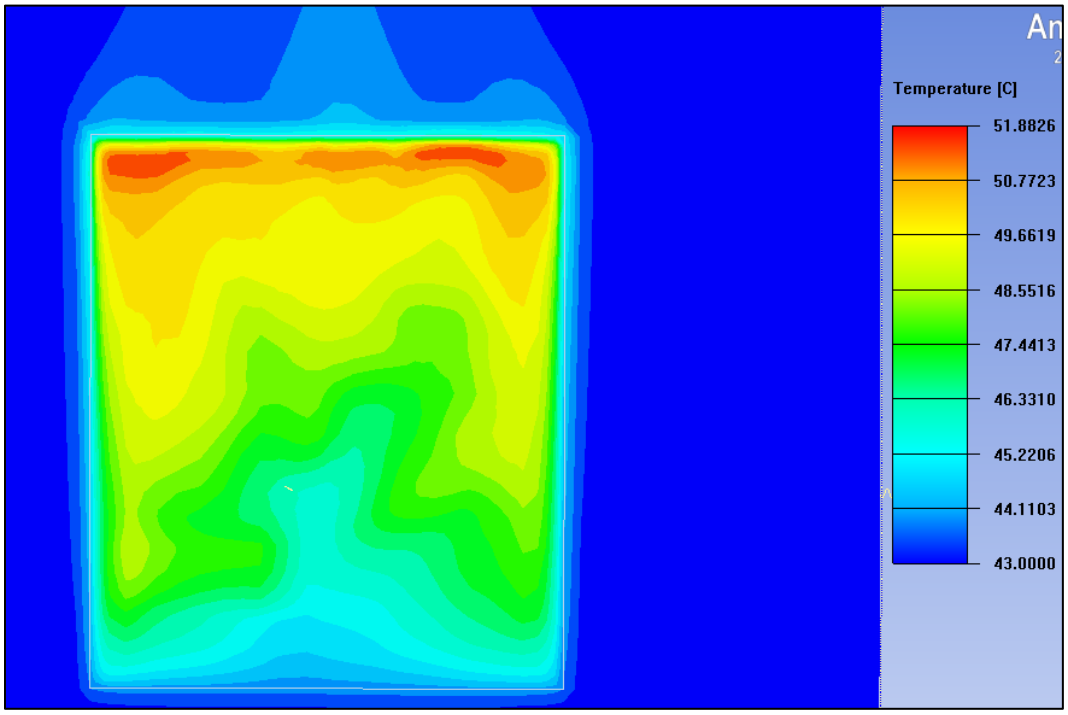

Figure 21: Thermal Simulation of Preselector in Extreme Temperature

An experiment was conducted to validate the simulation results. A prototype preselector equipped with temperature sensors was placed on the roof of MITRE's E-building in Bedford, MA, with direct exposure to sunlight. The ambient temperature reached a maximum of 27.8° C that day. While the internal temperatures fluctuated due to alternating periods of direct sunshine and cloud cover, the maximum recorded internal temperature was 8.3° C above ambient. This result closely matched the simulation and provided confidence in the thermal analysis.

The component in the preselector with the lowest temperature limit is the RF limiter, which has a maximum operating temperature of 50° C. Working backwards from this limit, and using the simulated temperature increase of 8.6° C, an ambient temperature of 41.4° C with full solar exposure would be required, for the internal temperature to reach this limit. It is unlikely that the sensors will experience such high temperatures in their intended deployment locations.

Temperature data from deployed preselectors confirms that internal temperatures, while occasionally approaching the limit, never reached or exceeded it. Figure 22 shows the internal temperatures recorded for several preselectors during the warmest months of 2025. This plot includes several preselectors deployed on the East Coast - Norfolk International Terminal (NIT) and Hampton University (HU) - and the West Coast - Midway Museum and Catalina. Additionally, it includes a preselector deployed as part of a development sensor at Green Mountain Mesa (GMM) in Boulder, CO. The plot spans a 2-month period and shows daily temperature variations resulting from the earth's diurnal cycle. During this period the maximum recorded internal temperature for any preselector was 46° C, which occurred at both East Coast sensors. The West Coast preselectors remained appreciably cooler. Data from the same months in the previous year, not included here, show similar results with slightly lower temperature peaks.

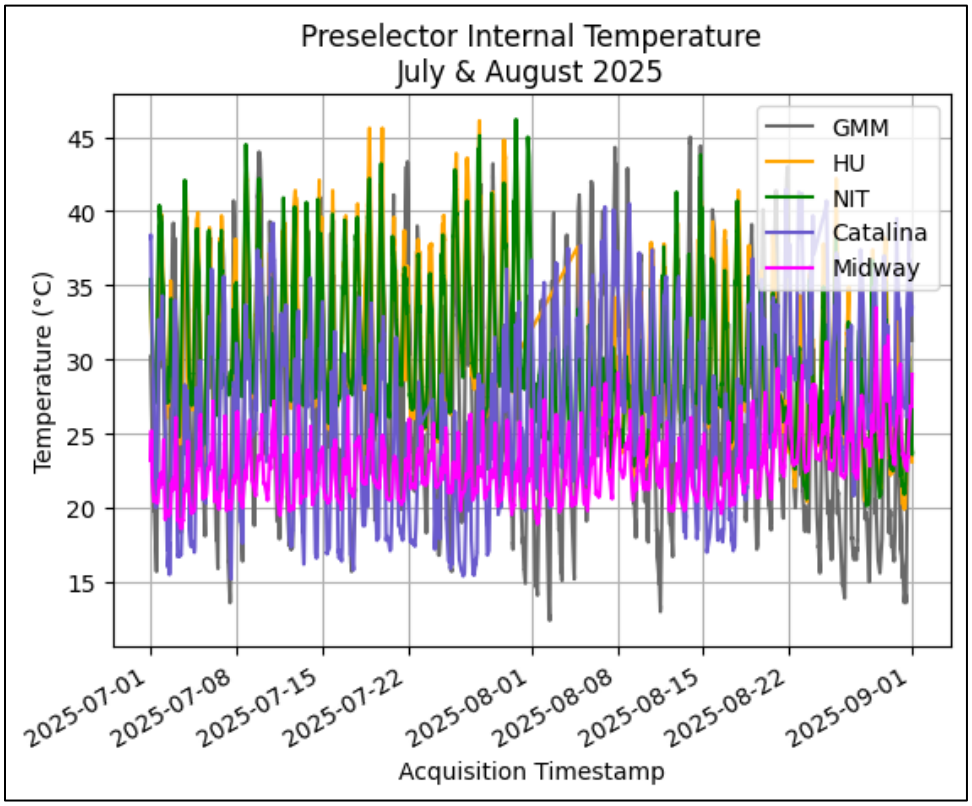

Figure 22: Internal Temperature Data for Deployed Preselectors, July-August 2025

3.3 SPU Assembly

The SPU assembly contains the remaining components in the RF signal path not included in the preselector; namely the attenuator, gain block amplifier and RSA. Additionally, it houses the embedded computer as well as various power management, system control, and networking components. A block diagram of the SPU is shown in Figure 23. Due to the overall size of the design, the power distribution and control portions were separated into sub-diagrams, labeled Figure 24 and Figure 25, respectively. Part numbers for the SPU's key components are provided in Table 5.

The RF input to the SPU is received from the preselector via a potentially long coaxial cable. Because sensor deployments vary significantly in cable length, external cable insertion loss may also vary widely. The attenuator immediately following the RF input is used to compensate for differences in cable loss by selecting a value that achieves a combined cable and attenuator insertion loss of 15 dB. Next, a gain block amplifier preceding the RSA provides additional gain needed to maintain a low overall system noise figure. Finally, the RSA converts the RF signal to a digital complex baseband signal, and the resulting IQ data is transferred to the embedded computer for processing via its USB 3.0 interface.

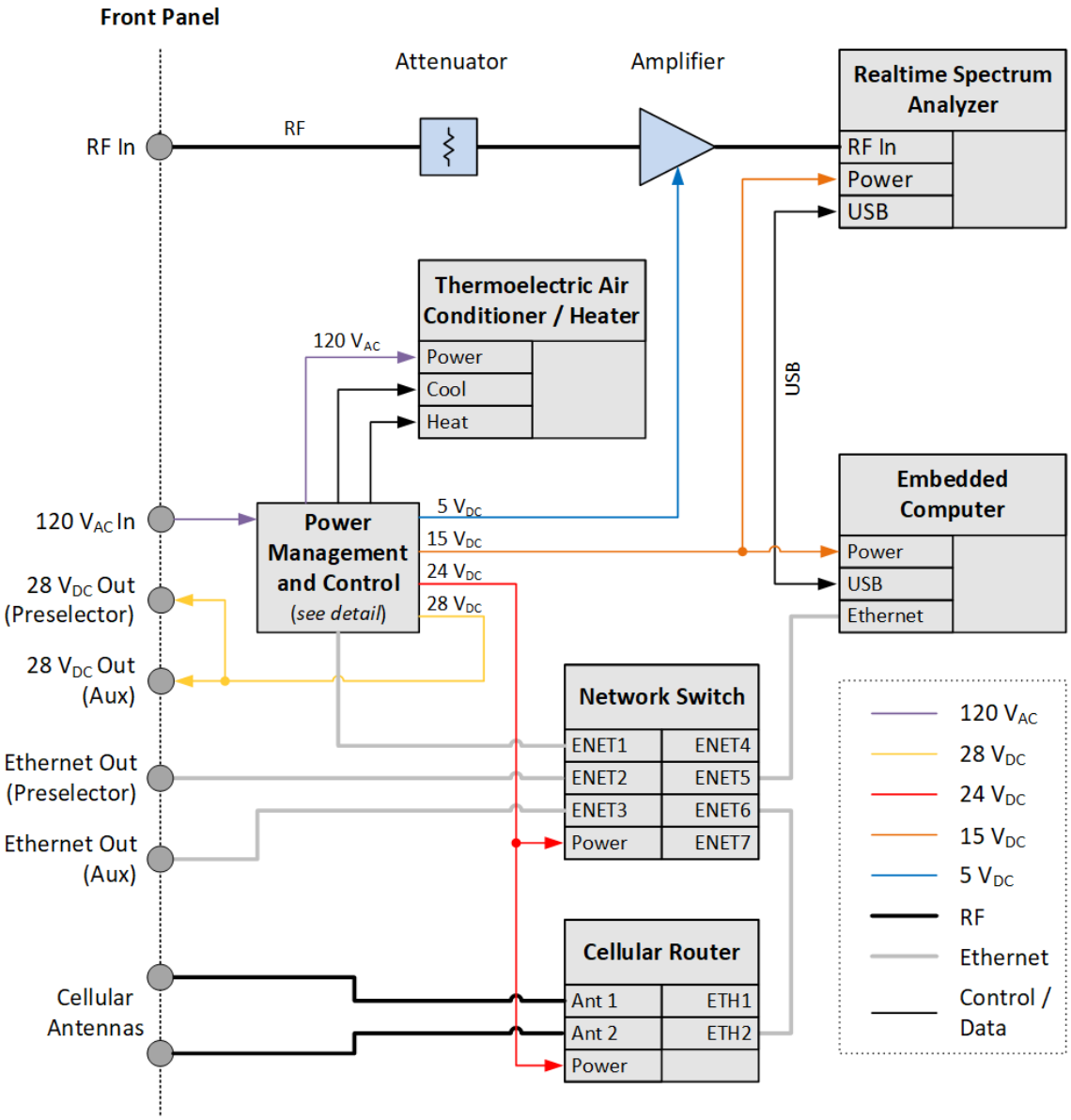

Figure 23: SPU Block Diagram

A cellular router provides remote access to the sensor, allowing retrieval of sensor data products as well as remote monitoring and administration. This mobile networking strategy enables sensor deployments in locations where wired network connectivity is unavailable but cellular coverage exists. The cellular router functions as both a cellular modem and network router, creating a local network for the sensor. In combination with the network switch, this setup enables Ethernet connectivity among the embedded computer, controller, and preselector.

Like the preselector, the SPU is housed in a sealed, weatherproof enclosure. However, unlike the preselector, some SPU generate significant heat. Therefore, a TEC has been included to ensure that internal temperatures remain within component operating limits. The TEC's active cooling enables the use of a higher-performance embedded computer to meet the sensor's processing demands. The specifications of the computer, summarized in Section 2.1.8, would not be possible with passive cooling. Further details regarding SPU temperature control are provided in Section 3.3.1.

The power management components in the SPU generate the required supply voltages and distribute power to the entire sensor, including the preselector. As shown in Figure 24, the sensor is powered by a standard 120 V_{AC} source. With the exception of the TEC, which operates directly from this supplied 120 V_{AC}, all components in the SPU operate with DC voltages. The 120 V_{AC} source is converted to 24 V_{DC} by a 240W power supply, which is then backed up by a 24 V_{DC} uninterruptible power supply (UPS). The UPS's 24 V_{DC} output is distributed directly to several components; the cellular router, network switch, controller, and three DC-DC converters. These DC-DC converters generate additional supply voltages for the remaining components, including 15 V_{DC} for the RSA and embedded computer, 5 V_{DC} for the amplifier and 28 V_{DC} for the preselector.

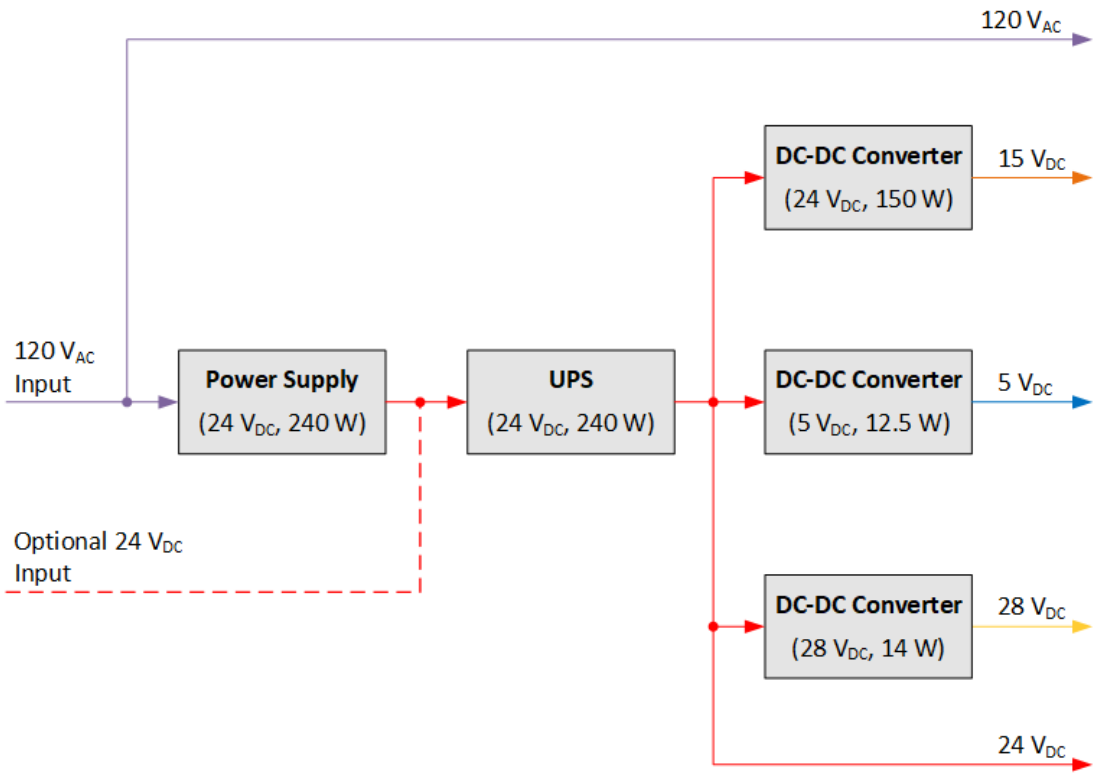

Figure 24: SPU Power Management Block Diagram

With a simple reconfiguration, the sensor can also be powered by an external 24 V_{DC} source. In this configuration, the 24 V_{DC} power supply is disabled, and the UPS receives power directly from the external source. However, it is important to note that the TEC cannot operate in this configuration, as it requires a 120 V_{AC} source. Therefore, this configuration is only suitable for moderate temperature environments where the TEC is not needed. Alternatively, the TEC vendor offers a DC-powered version that could be explored.[8]

A network-enabled controller, along with several expansion modules, performs a variety of system control and monitoring functions. Details of these controllers are shown in Figure 25.

Like the preselector, the main controller has a digital sensor interface that communicates with several external temperature and humidity sensors. These include a combined

[8] EIC ThermoTEC™ 140 Series – 400 BTU (DC), which operates from a 24-28 V_{DC} supply

temperature/humidity sensor placed centrally with the assembly, as well as two temperature sensors located near the air intake and exhaust of the TEC.

The main controller also interfaces with three expansion modules to provide additional capabilities. First, the dual high-current relay module controls the 15 V_{DC} supply voltage to the embedded computer. While power should always be supplied to the computer during normal operation, it's important to have the ability to remotely cycle power in the event of a system malfunction. The high-current relay module also controls the 120 V_{AC} supply voltage to the TEC, allowing it to be turned on and off as needed to maintain an appropriate temperature inside the enclosure.

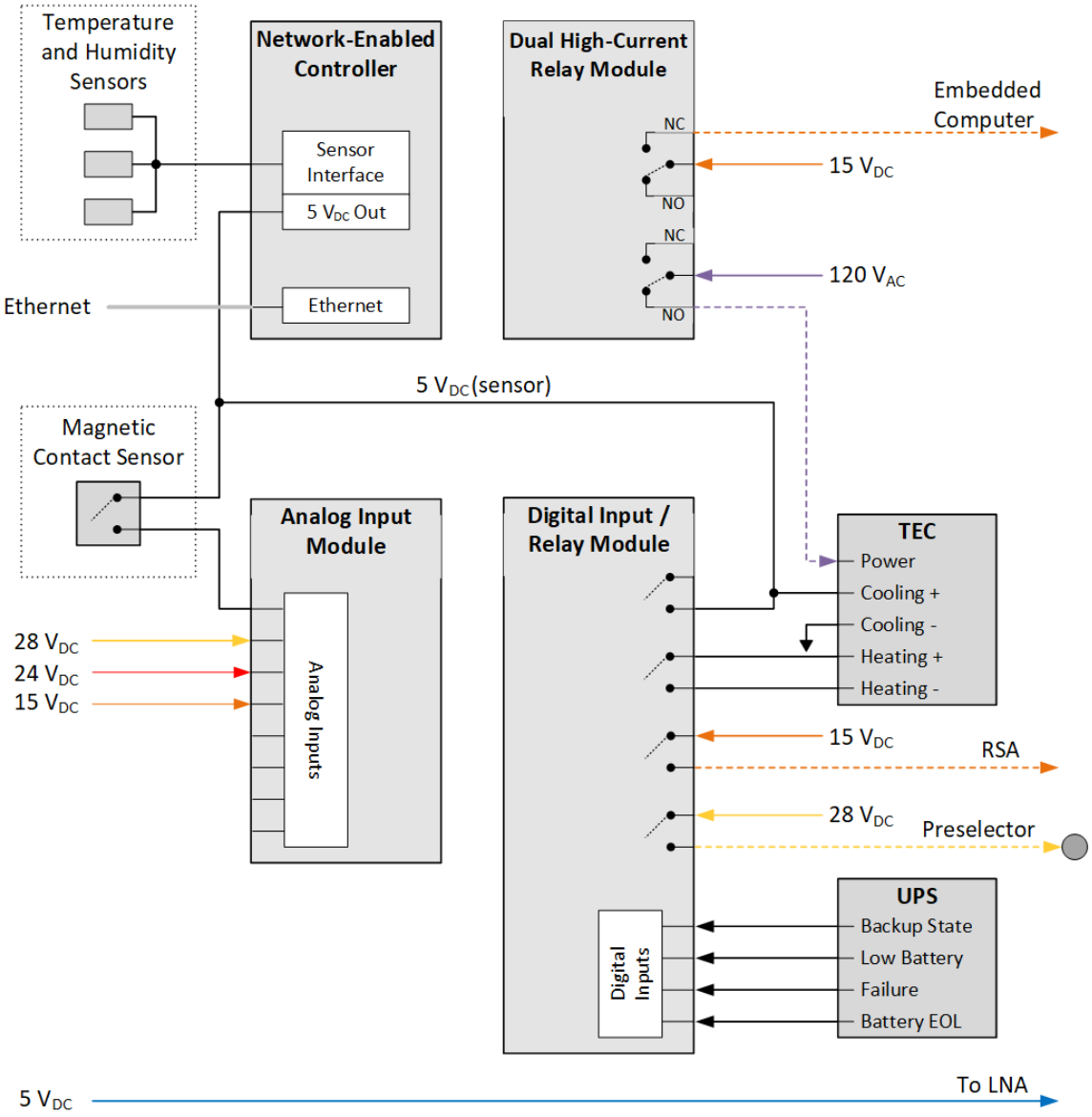

Figure 25: SPU Control and Monitoring Block Diagram

Next, the digital input / relay expansion module serves several purposes. Relays in this module control the 15 V_{DC} supply voltage for the RSA and the 28 V_{DC} supply voltage for the preselector. As with the computer, power to both the RSA and preselector is always enabled during normal operation, but the ability to remotely cycle power is important for maintenance and diagnostics. These relays also enable the cooling and heating modes of the TEC. Cooling mode is activated by setting the TEC's *Cooling*+ control signal to 5 V_{DC}, while heating is enabled by closing the circuit between the TEC's *Heating*+ and *Heating*- terminals.

The digital inputs on this expansion module monitor several UPS status and health indicators. These indicators alert the system when the primary power source is lost, when the backup battery is at a low state of charge, when a UPS failure is detected, or when the battery has reached end of life.

Finally, the analog input expansion module is used to remotely monitor various DC voltages in the system. It also monitors a magnetic contact switch that indicates when the SPU enclosure door has been opened. Although this is a 5V digital signal, no digital inputs remain, so an analog input was repurposed.

Table 5: SPU Component Part Numbers and Operating Temperature Ranges

Component	Manufacturer	Part Number	Temperature Range
Amplifier	Mini-Circuits	ZX60-83LN-S+	-40 to +85°C
Real time spectrum analyzer	Tektronix	RSA507A	-10 to +55°C[9]
Small form factor computer	Simply NUC	NUC13TZi7	-40 to +60°C
Cellular router	Digi	IX20-W007	-40 to +70°C
Network switch (8-port)	TRENDnet	TI-G80	-40 to +75°C
Thermoelectric 400 BTU cooling and heating unit	EIC	AAC-140C-4XT-HC-RC	+60°C[10]
Network-enabled controller	ControlByWeb	X-400-I	-10 to +85°C
Controller 4-relay, 4-input expansion module	ControlByWeb	X-17s	-40 to +65°C
Controller analog input expansion module	ControlByWeb	X-22s	-40 to +50°C
Controller dual high-current relay expansion module	ControlByWeb	X-11s	-40 to +65°C
Power supply ($24V_{DC}$)	Omron	S8VK-X24024A-EIP	-40 to +70°C
UPS ($24V_{DC}$)	Omron	S8BA-24D24D240LF	0 to +55°C
DC-DC converter (15VDC)	Traco	TEP 150-2413WI	-40 to +70°C
DC-DC converter (5VDC)	Acopian	24EB5E250	-20 to +70°C
DC-DC converter (28VDC)	Acopian	24EB28E50	-20 to +70°C

[9] Operating temperature without battery installed. RSA battery is not included when installed in SPU because SPU has its own full-system uninterruptible power supply.

[10] No minimum operating temperature specified.

The SPU is housed in a 63 cm x 53 cm x 25.5 cm fiberglass-reinforced polycarbonate weatherproof enclosure with a NEMA 4X / IP67 rating. Like the preselector, this enclosure was selected to protect the internal electronics from the environmental conditions expected in locations where the sensor is intended to be deployed, including precipitation, solar radiation, and corrosive sea spray. Due to the heat generated by the internal components and the lack of air-flow in the sealed enclosure, the TEC is needed to prevent internal temperatures from exceeding operating limits. The TEC also provides heating to prevent the internal temperature from falling below the operating range in extremely cold temperatures. Further details on thermal control and testing are provided in Section 3.3.1.

All RF and electrical components are mounted on series of aluminum brackets and plates, which are then mounted to a main base plate. A photo of the internal assembly is shown in Figure 26. The RSA, located under the baseplate and out of view, has been removed from its ruggedized enclosure prior to mounting to conserve space.

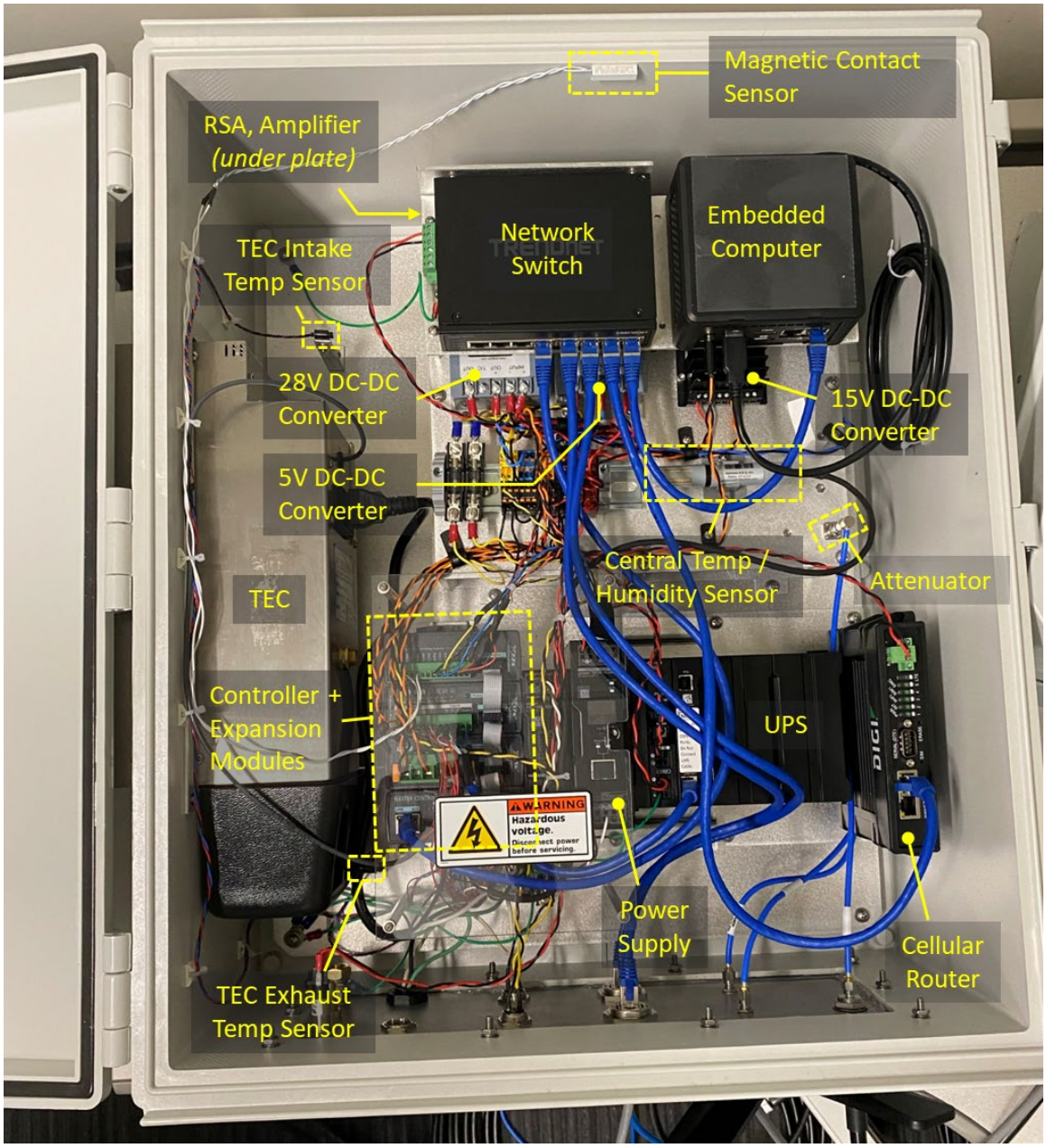

Figure 26: Annotated Photo of SPU Assembly

The bottom side of the enclosure is modified with a connector panel, shown in Figure 27, featuring feed-through connectors for the RF input, cellular antennas, Ethernet and 28 V_{DC} power output to the preselector. A power cord with a standard NEMA 15-5 plug connects to a 120 V_{AC} receptacle, and a DC input connector can optionally supply power to the SPU from an external 24 V_{DC} source.

Figure 27: SPU Connector Panel

Figure 28 shows a photo of a SPU deployed at the CBBT sensor site in October 2024. The SPU is mounted on the parapet on the roof of the Island 4 maintenance building. Next to the SPU, the cellular antenna is mounted on a short mast, just high enough to clear the parapet. The loop of cable below the SPU is a service loop for the long coaxial cable, DC power cable, and Ethernet cable that run to the preselector (refer to Figure 20).

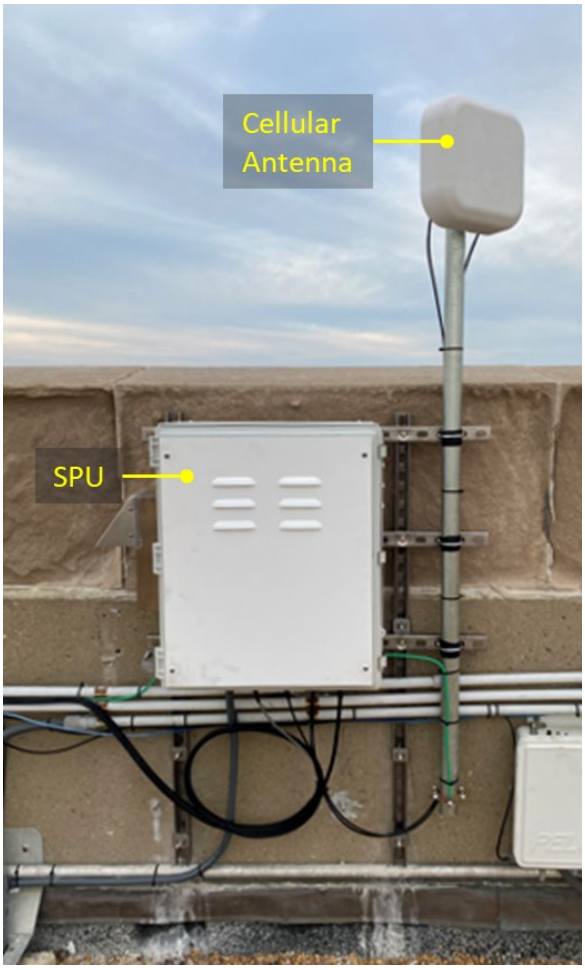

Figure 28: SPU Mounted to Parapet on Roof of Chesapeake Bay Bridge-Tunnel Island 4 Maintenance Building

3.3.1 SPU Thermal Control and Testing

The SPU includes a thermoelectric cooling and heating unit to maintain internal temperatures within the components' operating ranges, even during extreme ambient conditions. The TEC cools the enclosure without exchanging external air, keeping it sealed and protected from the moist and corrosive environments expected at deployment sites. The TEC, with a specified cooling capacity of 430-560 BTU/hour, was selected to maintain an internal temperature of no more than +50 °C with an ambient temperature of up to 43.3 °C, which is the maximum expected temperature based on MIL-HDBK-310.

The TEC is controlled by the SPU's internal system controller and can be set to one of four operating states. First, the TEC can be completely powered off, to maximize its operating life, or to eliminate fan noise where noise is a concern. Second, the TEC can be powered on without cooling or heating enabled; in this state, it simply runs its internal fans to circulate air within the enclosure. Third and fourth, the TEC can operate with either cooling or heating enabled. A script running on the SPU controller monitors the internal temperature and sets the TEC operating state according to predetermined setpoints.

The SPU was tested in a temperature chamber to validate the design and determine the appropriate TEC control setpoints. During the test the SPU was fully powered, with its internal components self-heating as they would during normal operation. Table 6 lists the setpoints used for this test. These setpoints include 2 °C hysteresis to prevent excessive cycling of the TEC operating states near the temperature thresholds.

Table 6: SPU Temperature Control Setpoints

	Cold Temperature Setpoints		Warm Temperature Setpoints	
	TEC Power	**Heating Mode**	**TEC Power**	**Cooling Mode**
Enable	<8 °C	<5 °C	>42 °C	>45 °C
Disable	>10 °C	>7 °C	<40 °C	<43 °C

For the first test, the SPU was operated in the temperature chamber while the TEC was powered off. The ambient temperature started at 0 °C and was increased in 10 °C increments to determine the maximum ambient temperature at which active cooling is not required. During the test, temperatures were recorded at three sensors inside the SPU, as well as the ambient temperature. The three SPU temperature sensors were the central temperature sensor, TEC intake temperature sensor, and the TEC exhaust temperature sensor (see Figure 26 for temperature sensor locations). The resulting temperature data are shown in Figure 29.

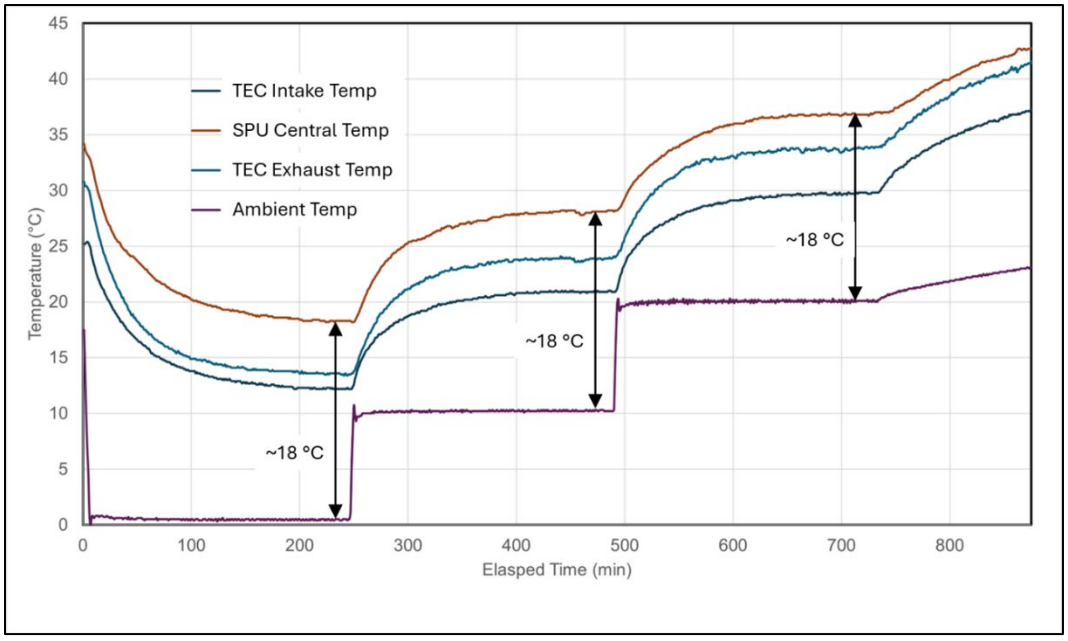

Figure 29: SPU Temperature Test with TEC Disabled

This test shows that, with the TEC disabled and no air circulation inside the SPU, the highest temperature occurs near the central temperature sensor. This is expected, as that sensor is located where warm exhaust air from the embedded computer is discharged. The test also shows that the highest temperature reading settles to approximately 18 °C above the ambient temperature.

Given that the maximum internal temperature should not exceed 50 °C, this suggests the SPU can operate at ambient temperatures up to approximately 32 °C without the TEC. However, this test does not account for exposure to solar radiation, which would result in a greater difference between the internal and ambient temperatures and further limit the temperature range over which the SPU can operate without the TEC.

The next test, shown in Figure 30, evaluated the TEC's ability to maintain an acceptable internal temperature during periods of high heat and demonstrated the proper functioning of the TEC control script. This test began with an ambient temperature of 43 °C. As internal temperatures rose, the TEC remained off until the SPU central temperature reached 42 °C approximately 65 minutes into the test. At this threshold, as specified in Table 6, the controller activated TEC power, indicated by the yellow shading in the figure. The TEC fans circulated air inside the enclosure, but without active cooling, the temperatures continued to rise. When the central temperature reached 45 °C, about 75 minutes into the test, the controller enabled cooling mode, as indicated by the blue shading, and internal temperatures began to drop. When the central temperature fell to 43 °C, cooling mode was disabled, temperatures began to rise again, and the cycle repeated. During these cycles the internal temperature measured at the TEC exhaust peaked at approximately 51 °C, slightly above the target temperature. However, this test demonstrated that the TEC, when cooling was enabled, had sufficient capacity to maintain the required internal temperature. Using slightly more aggressive controller setpoints would keep temperature peaks under 50 °C.

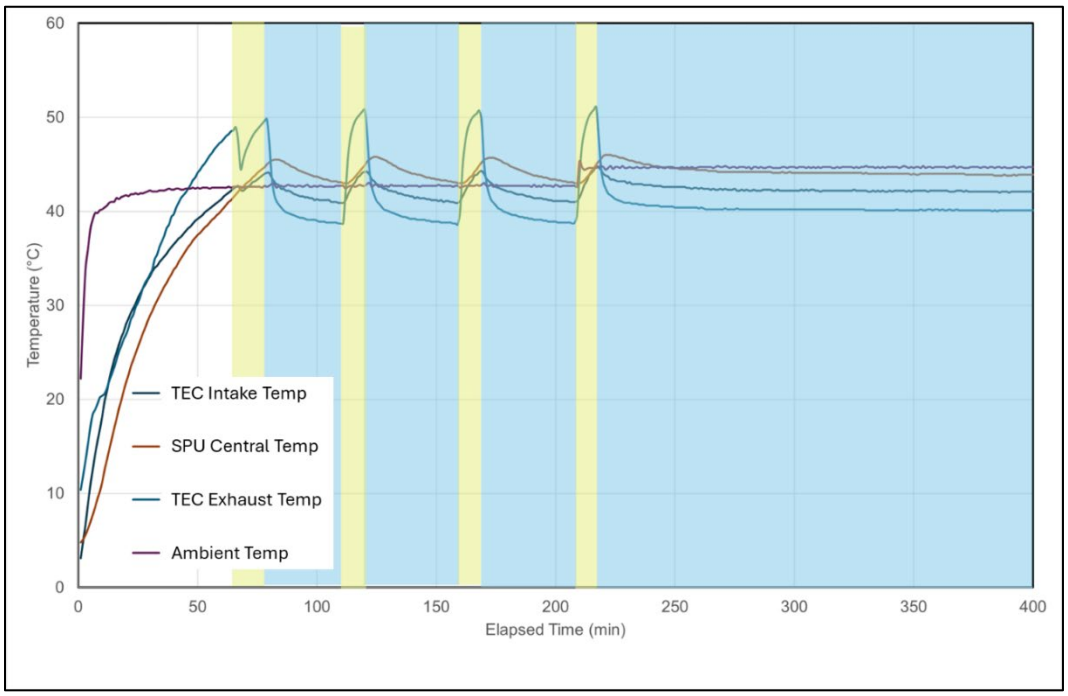

Figure 30: SPU High Temperature Test

At approximately 220 minutes into the test, the ambient temperature was increased to 45 °C. At this point, the controller enabled cooling mode again, which remained active because the internal temperature never dropped below the threshold required to disable it. During this period of continuous TEC cooling, the internal temperatures reached a steady state. The highest internal temperature, measured at the central sensor, was approximately 1 °C below the ambient temperature. Although the sensor is not expected to be exposed to such high ambient

temperatures, this result demonstrates that the TEC has sufficient cooling capacity and provides confidence that, even when the SPU is exposed to solar radiation, it should be able to maintain an acceptable internal temperature.

The final temperature chamber test, shown in Figure 31, exposed the SPU to low ambient temperatures and examined the ability of the TEC's heater to maintain an acceptable internal temperature. While the sensor is not expected to encounter extreme cold, it is useful to understand the minimum ambient temperature that can be tolerated. The minimum internal SPU temperature is limited by the UPS, which has a specified minimum operating temperature of 0 °C.

For this test the ambient temperature began at -5 °C, but internal temperatures did not fall to the thresholds needed to enable the TEC. The ambient temperature was then reduced to -15 °C, and at approximately 145 minutes into the test the SPU central temperature reached 8 °C. At that threshold, as specified in Table 6, the controller turned on the TEC power, indicated by the yellow shading, and air began circulating internally. Internal temperatures continued to fall, and when the central temperature reached 5 °C at approximately 150 minutes, the controller enabled heating mode, indicated by the red shading. At this point, internal temperatures began to rise, and when the central temperature reached 7 °C heating mode was disabled and temperatures began to fall again. The cycle repeated several times, and during these cycles, the internal temperature measured at the TEC intake reached minimums of approximately 0 °C.

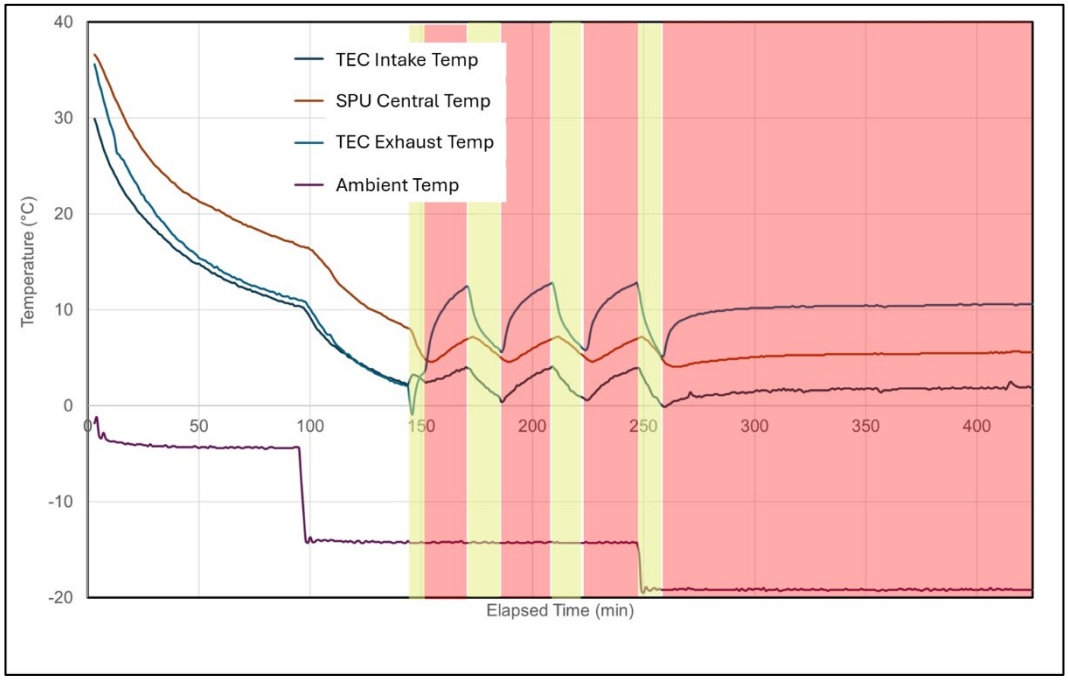

Figure 31: SPU Low Temperature Test

At approximately 250 minutes into the test the ambient temperature was reduced to -20 °C. At this point the controller enabled heating mode again, which remained active because the internal temperature never rose above the threshold required to disable it. During this period of continuous TEC heating, the internal temperatures reached a steady state and the lowest internal temperature, measured at the TEC intake, was still slightly above the required minimum at 2 °C.

This demonstrates that the SPU is able to operate in ambient temperatures down to -20 °C, even though it is not expected to be exposed to such low temperatures.

Temperature data from several deployed SPUs confirm that the integrated temperature controller operates as expected and that the TEC is able to maintain an acceptable internal temperature during the warmest period of the year. Figure 32 shows the internal temperatures recorded for three SPUs during July and August 2025. One of these SPUs - CBBT - is deployed on the East Coast, while another – Catalina - is deployed on the West Coast. The figure also includes temperature data for the SPU deployed with the development sensor at GMM in Boulder, CO.

During this period the internal temperature never exceeded 47° C for any of these SPUs, demonstrating that the TEC has sufficient cooling capacity for the sites at which the sensor is deployed. Furthermore, a close examination of the hourly temperature trends within this data indicates that the temperature controller is operating as expected. During the warmest days, and in particular during the warmest hours within those days, internal SPU temperatures cycled between approximately 42° C and 46° C. This closely aligns with the temperature control thresholds at which the TEC cooling mode is enabled and disabled, indicating that the controller is cycling the TEC cooling mode as intended.

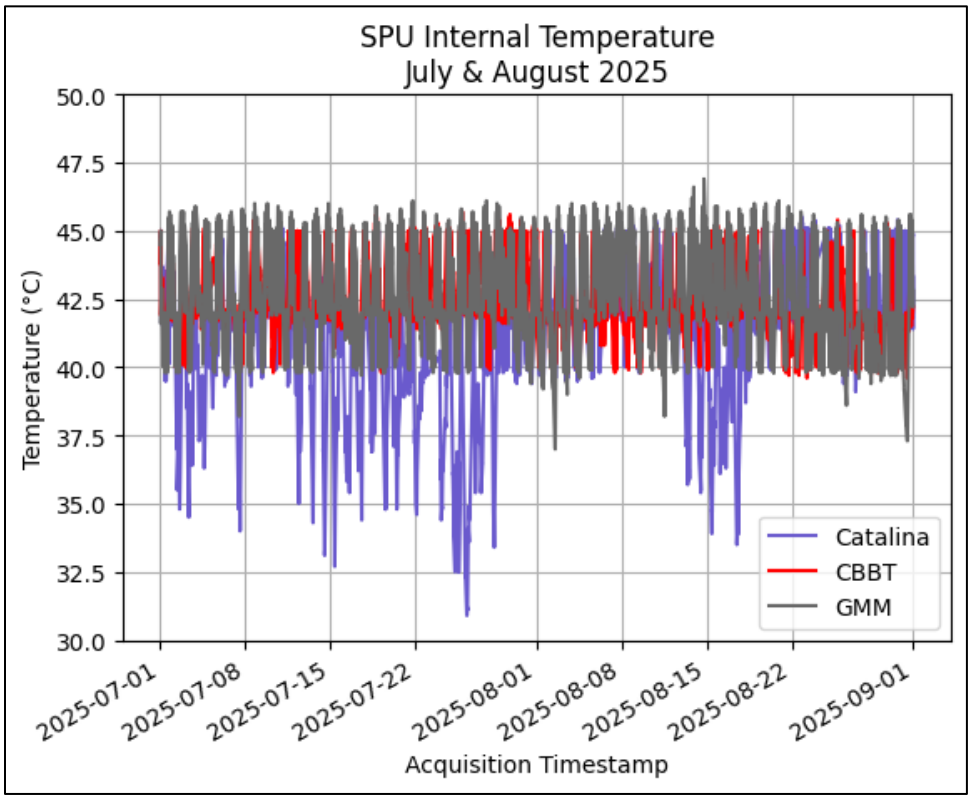

Figure 32: Internal Temperature Data for Deployed SPUs, July-August 2025

While most of the sensors are deployed in locations where only TEC cooling is needed, the sensor at GMM has been exposed to extremely cold temperatures and has demonstrated the TEC heating capacity. The Boulder, CO area experienced a cold wave from 13-16 January 2024 where ambient temperatures fell below -20° C. In response, the SPU at GMM periodically

enabled the TEC heating mode to maintain an acceptable internal temperature as shown in Figure 33 This data shows variation in temperature throughout the days, with the TEC heater cycling on and off during colder periods. Heater operation is evident in the rapid temperature swings between approximately 5° C and 8° C, which align with the temperature controller thresholds for enabling and disabling heating mode. When enabled, the heater had sufficient heating capacity to raise the internal temperature, and throughout the entirety of this cold period the internal temperature never fell below the minimum acceptable temperature of 0° C.

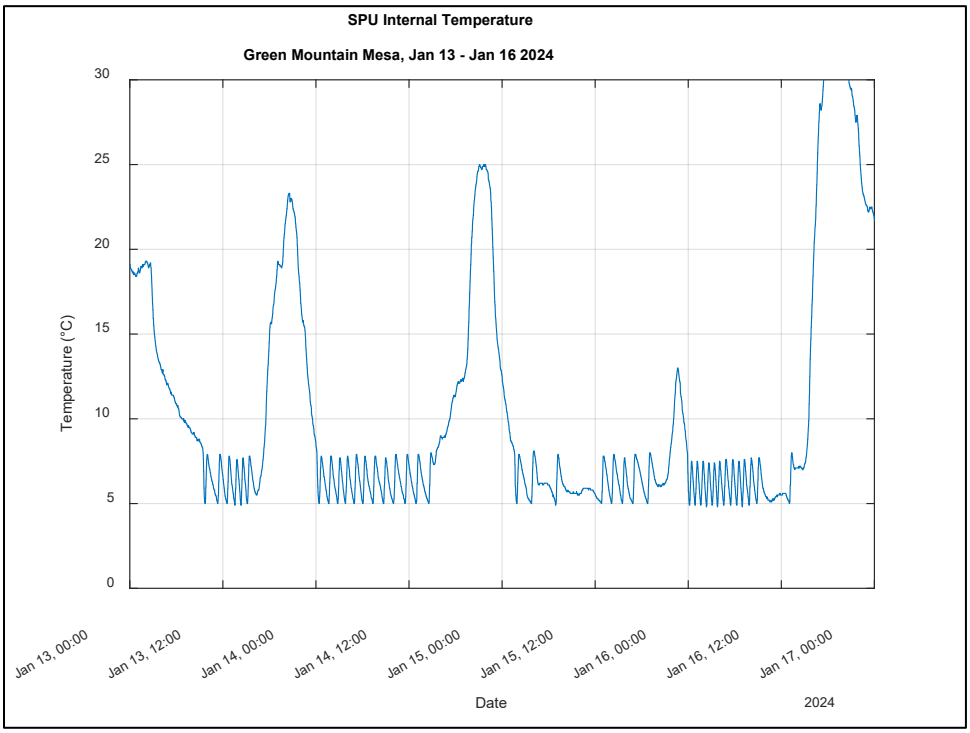

Figure 33: Internal Temperature Data for GMM SPU, January 13-16, 2024

4 System Measurements

Various measurements were performed on the fully integrated SEA sensor, including total power consumption and several RF system measurements. These measurements were conducted on the complete system, except for the external antennas. Additionally, a 10 dB attenuator replaced the long coaxial cable between the preselector and SPU, and a 5 dB attenuator was installed inside the SPU. While the length of the coaxial cable will vary for deployed sensors due to site specific conditions, the attenuator in the SPU will be adjusted as needed to achieve the same combined cable and attenuator insertion loss as used for these tests.

Details of these measurements are presented in the following subsections.

4.1 Power Consumption

Total power consumption was measured at the system's 120 V_{AC} input while the sensor operated in a typical state, ensuring the computational load on the embedded computer was representative of a deployed sensor. Measurements were taken with the TEC in various operating states, as TEC activity significantly affects total power consumption and varies according to environmental conditions at the sensor site. The results are presented in Table 7.

Table 6: Sensor Power Consumption

TEC State	Typical Power	Maximum Power
Off	85 W	100 W
On (fan only)	100 W	115 W
Cooling	270 W	310 W
Heating	210 W	230 W

4.2 Gain and Noise Figure

Full system gain and noise figure are measured as part of the sensor's routine calibration process. Details of this process are outside the scope of this document, but can be found in the NIST publication "Noise Based Power Calibration Techniques for Mid-band Radio Frequency Sensors" [2].

Gain and noise figure measurements during calibration uses the preselector's built-in noise source and follow the widely used Y-factor method. For this measurement, the RF switches in the preselector are configured to select the noise source as the system input. IQ data is acquired from the RSA with the noise source both enabled and disabled, and the mean power is computed from the IQ time series. These mean power measurements, along with the excess noise ratio (ENR) of the noise source, are used to calculate system gain and noise figure. A full explanation of the measurement technique and calculations can be found in the application note, *The Y Factor Technique for Noise Figure Measurements* [7]. This process is repeated at 18 frequencies, covering the 15 measurement channels within the CBRS band and several frequencies outside the CBRS band. Gain and noise figure results for the five sensors are shown in Figure 34.

These measurements were performed with a fixed RSA reference level of -25 dBm and attenuator value of 0 dB, which is the typical deployment configuration. These settings are relevant because they affect the noise figure of the RSA as shown in Figure 12, and therefore impact the overall system noise figure.

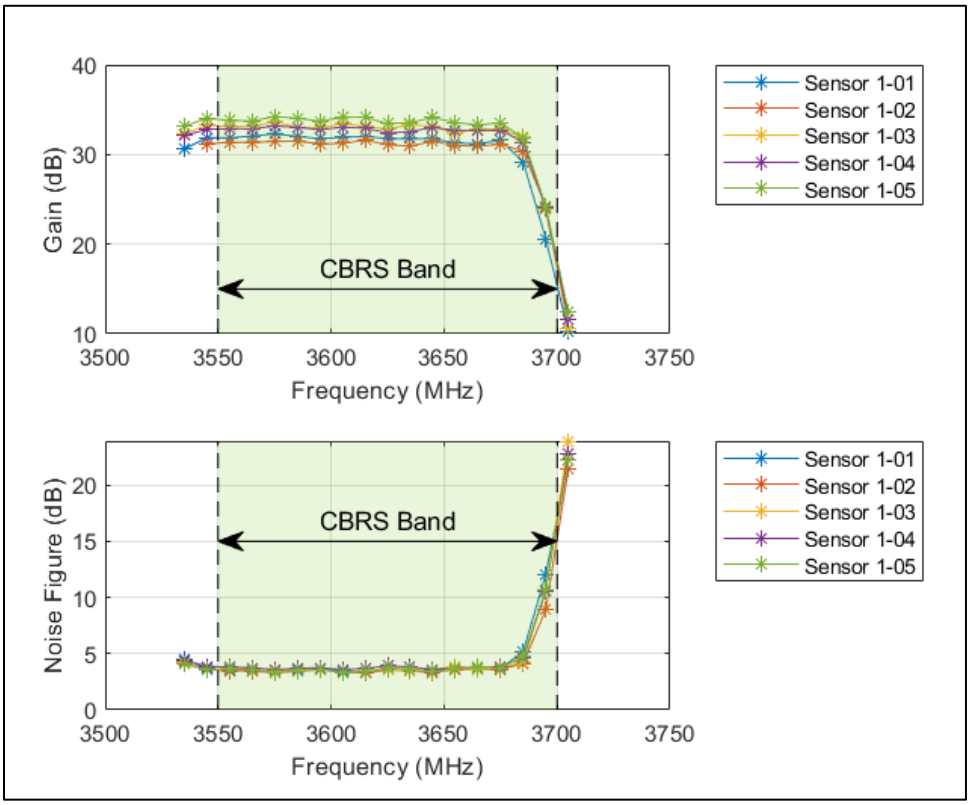

Figure 34: Full System Gain and Noise Figure

As shown in the upper subplot of Figure 34, the measured gain of each individual sensor varies by less than 0.75 dB across the CBRS band, except for the upper two channels. The gain begins to roll off in the measurement channel centered at 3685 MHz and then falls sharply in the channel centered at 3695 MHz. This response is expected and closely follows the insertion loss of the bandpass filter, as shown in Figure 6.

Across the five sensors, a gain variation of approximately 3 dB is observed. It is important to note that the RSAs integrated into the sensors are included in these measurements, and thus the results are affected by the accuracy of the RSAs. The RSAs have a specified accuracy of ±1.75 dB for the frequency range at which this measurement is performed, which likely accounts for much of the variation observed across sensors. To a lesser extent, differences in insertion loss of the RF components among sensors also contribute. Regardless, correction factors determined for each individual channel during the calibration process are applied to the measurement data to compensate for these variations.

The measured system noise figure, shown in the lower subplot of Figure 34, is just under 4 dB for all measurement channels within the CBRS band except for the upper two channels. Similar to the gain measurement, the noise figure degrades slightly in the channel centered at 3685 MHz

and then increases sharply in the channel centered at 3695 MHz, which is a direct result of the insertion loss roll-off of the bandpass filter at those frequencies.

Both the gain and noise figure measurements closely match the simulated results, shown in Figure 5.

4.3 Wideband Frequency Response

The gain measurement presented in the previous section was limited to the frequency range over which the calibration process is performed. That measurement shows the gain variation across the specific measurement channels but does not show the wideband frequency response of the sensor. A different measurement technique was performed to determine the wideband frequency response.

For this measurement, a signal generator was used to source a CW test signal at the input of the preselector. The source signal was swept over the frequency range 3375 to 3875 MHz in 1 MHz steps, and at each frequency step the measured spectrum trace was acquired from the RSA. System gain was then determined from the difference between the signal level measured by the RSA and the known signal level at the input. The resulting measurement for one sensor is shown in Figure 35.

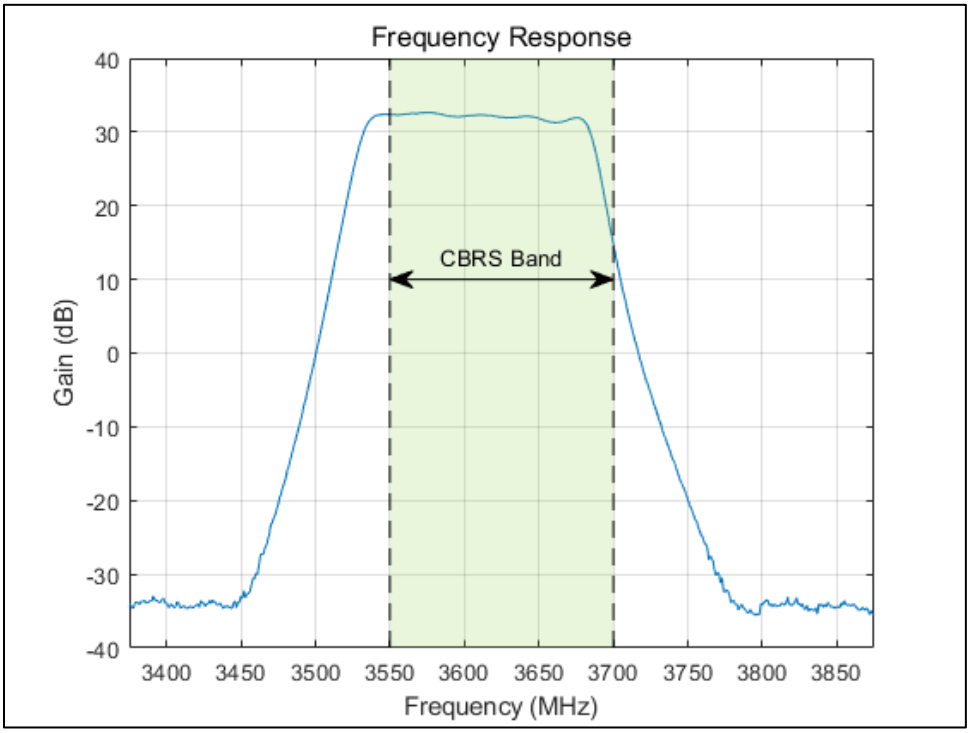

Figure 35: Full System Frequency Response

As with the previous gain measurement, this measurement shows a system-level response that closely follows the response of the bandpass filter. However, it extends farther beyond the limits of the CBRS band and provides additional insight into the sensor's ability to reject out-of-band emissions.

4.4 Maximum Input Power

The maximum input power of the sensor was measured using the same procedure described in Section 2.1.6, except that the measurement was performed on the full sensor system rather than just the RSA and over a range of frequencies rather than at a fixed frequency. As with to the RSA measurement, the maximum input power here is defined as the highest input power at the preselector input that *does not* cause an ADC overrange condition in the RSA.

For this measurement, the RSA reference level was set to -25 dBm and the input attenuator was set to 0 dB, which is the typical deployment configuration and same settings used for the full system gain and noise figure measurements. As with the gain and noise figure measurements, this measurement was performed at 18 frequencies, covering the 15 measurement channels within the CBRS band as well as several frequencies outside the band. The results are shown in Figure 36.

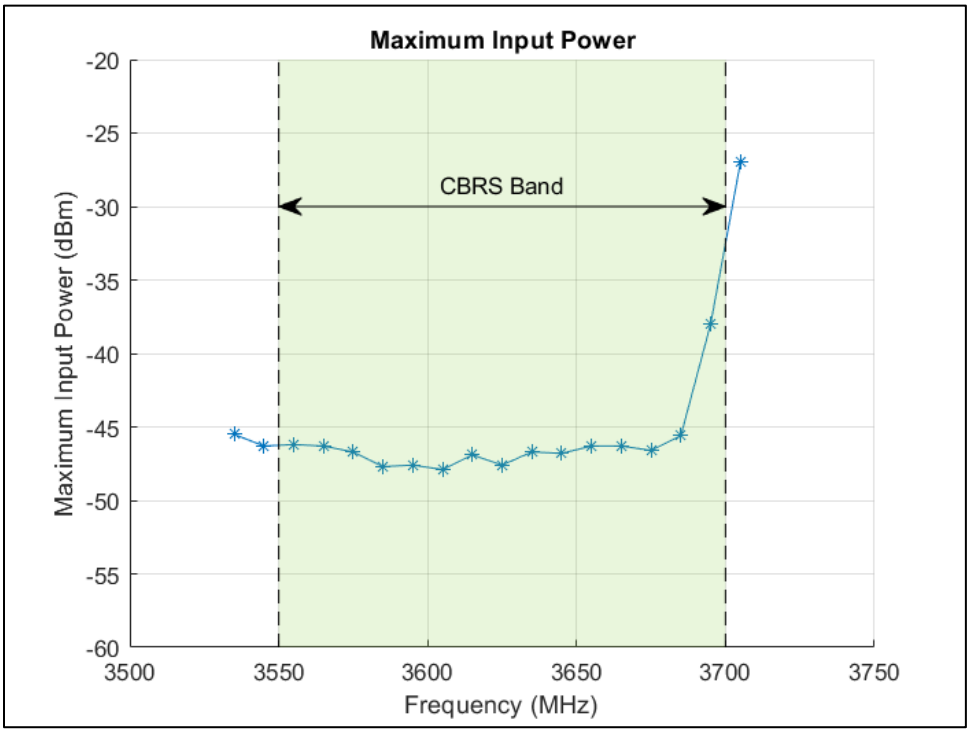

Figure 36: Full System Maximum Input Power

The maximum input level ranges from -48 dBm to -46 dBm at all frequencies within the CBRS band, except for the upper two channels. As with the previous measurements, the insertion loss of the bandpass filter affects the measurement results in the upper two channels. In this case, the increased insertion loss in the upper channels allows the sensor to tolerate a stronger input signal.

4.5 Dynamic Range

The dynamic range of the full sensor was measured at the center of the CBRS band using the same procedure that was used to measure the RSA only in Section 2.1.7. First, DANL and maximum input power of the full sensor were measured with a fixed RSA center frequency of 3625 MHz and a range of RSA reference level and attenuator settings. From each of these DANL measurements the total power in a 10 MHz measurement channel was derived, and this was combined with the maximum input power to determine dynamic range. The result is shown

in Figure 37. Blue lines in the plot indicate measurements where the RSA attenuator value was offset from the reference level by 25 dB, while orange points indicate measurements where the attenuator was fixed at its lower limit of 0 dB and therefore was offset by less than 25 dB from the reference level.

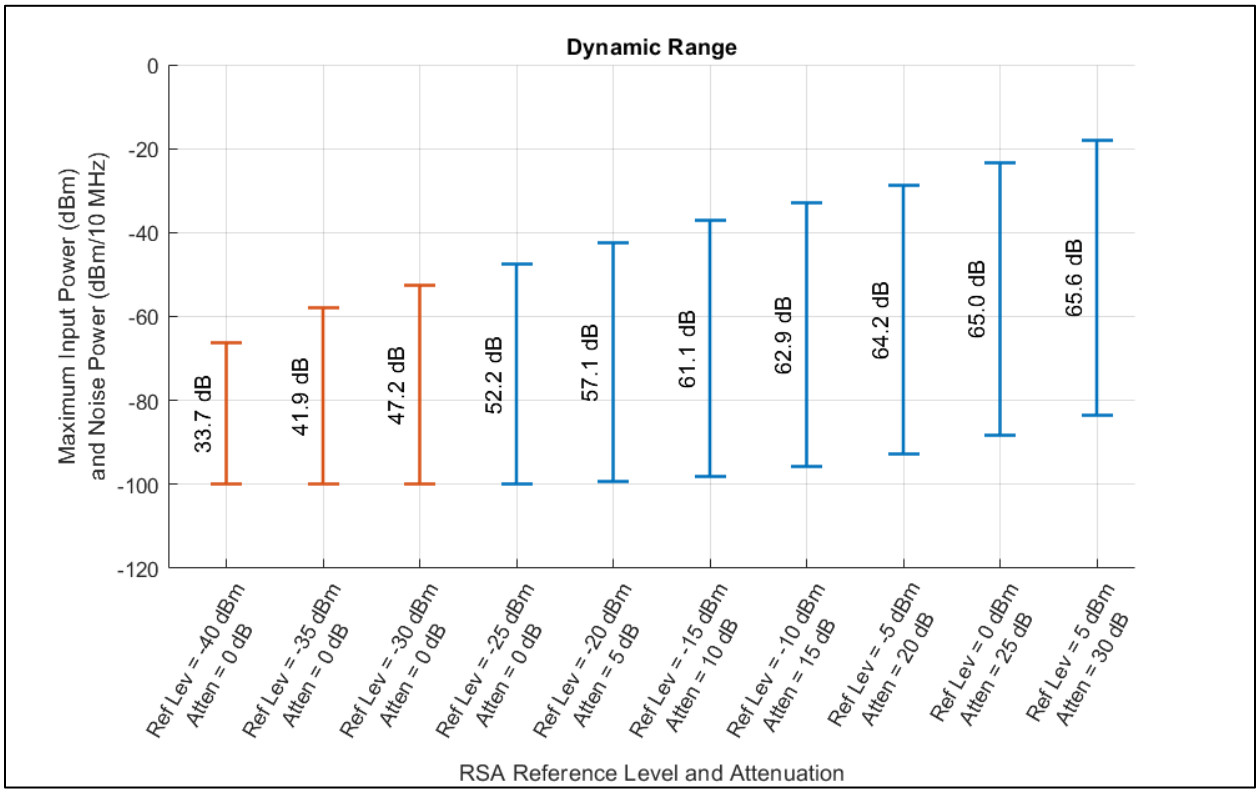

Figure 37: Full System Dynamic Range for Various Reference Level and Attenuator Settings

This figure demonstrates the configurability of the sensor to enable measurement of various ranges of input signal levels. Furthermore, these settings can be configured on a per-channel basis, allowing the input ranges to be tailored to the RF environment. The figure also illustrates the trade-off between sensitivity and dynamic range. The reference level and attenuator settings can be configured to increase sensitivity, but at a certain point the improvement to sensitivity becomes negligible while the degradation to dynamic range is significant.

5 Conclusion

The CBRS SEA sensor was designed to measure RF emissions in the United States 3550–3700 MHz CBRS band. The sensor was developed to enable a NASCTN study examining the effectiveness of the FCC's spectrum sharing methodology employed in that band. The sensor incorporates a modular architecture that optimizes RF performance while ensuring flexibility and ease of deployment. Smaller, low-power RF front-end components including the preselect filter, limiter, LNA and calibrated noise source are partitioned into the preselector assembly that can be installed in close proximity to the antenna, minimizing antenna cable loss and hence overall system noise figure. Larger, heavier and more power-consuming components including the embedded computer, RSA, power management, control and networking components are assembled into the SPU which can be installed in less constrained areas. Both assemblies utilize sealed enclosures to enable deployment in areas exposed to the weather. The preselector is passively cooled, while the SPU employs a TEC to maintain an appropriate internal operating temperature.

Features of the sensor include support for up to two external antennas, allowing both omnidirectional and directional measurements. Its built-in noise source enables periodic self-calibration to ensure accuracy and long-term stability of measurements. It uses a custom-designed preselect filter, which has been intentionally rolled off near the upper edge of the CBRS band to protect against strong adjacent C-band 5G emissions. Finally, it is remotely monitored and managed through a cellular router and network-enabled controller.

System test results demonstrated performance and operational readiness, confirming suitability for collecting accurate RF data in support of the NASCTN study. As of the time of publication of this report, eight sensors are deployed and are operational.

A complete documentation package is available upon request to NASCTN@nist.gov that contains the schematics, assembly drawings and parts lists needed to reproduce the design.

6 References

[1] National Advanced Spectrum and Communications Test Network, "CBRS Sharing Ecosystem Assessment," [Online]. Available: https://www.nist.gov/programs-projects/cbrs-sharing-ecosystem-assessment. [Accessed 19 11 2025].

[2] A. Sanders, T. Schumann, D. Gu, K. Forsyth and X. Lu, "Noise Based Power Calibration Techniques for Mid-band Radio Frequency Sensors," 2025.

[3] D. Boulware, J. Haze, A. Romaniello, R. Ballard, B. Eales and T. Schumann, "Software Implementation for Citizens Broadband Radio Service Sharing Ecosystem Assessment (Forthcoming)," 2025.

[4] A. Sanders, A. Romaniello, D. Kuester, T. Schumann and A. Wunderlich, "Citizen's Broadband Radio Service (CBRS) Sharing Ecosystem Assessment (SEA) Sensor Data Manual," 2025.

[5] M. Cotton, L. Vu, B. Eales and A. Hicks, "3.45–3.65 GHz Spectrum Occupancy from Long-Term Measurements in 2018 and 2019 at Four Coastal Sites," 2020.

[6] Department of Defense, "MIL-HDBK-310: Global Climatic Data for Developing Military Products," 1997.

[7] Rohde & Schwarz, "The Y-Factor Technique for Noise Figure Measurements," 2021.

Appendix A RF Component Operating Frequency Ranges

The NASCTN CBRS SEA sensor was designed to operate in the 3500 MHz – 3700 MHz CBRS band, and the RF components were selected to support that specific frequency range. However, many of the RF components have wide operating frequency ranges, so with small modifications the sensor could be adapted to enable measurements in other bands. Table A-1 provides a summary of the component part numbers and operating frequency ranges, and the frequency ranges are presented graphically in Figure A-1. For context, the green shaded region in the figure represents the CBRS band.

Table A-1. Sensor RF Component Operating Frequency Ranges

Component	Manufacturer	Part Number	Frequency Range
Omnidirectional Antenna	L-com	HG3509U-PRO	3400 MHz – 3700 MHz
Directional Antenna	KP Performance Antennas	KP-3DPFP20	3500 MHz – 3800 MHz
RF Switch	Dow-Key	401-6308	DC – 18000 MHz
Noise Source	Keysight	346B-100	10 MHz – 18000 MHz
Isolator	Centric RF	CI2040	2000 MHz – 4000 MHz
Bandpass Filter	Reactel	8C7-3610-X180S11	3530 MHz – 3690 MHz
Limiter	Fairview	FMLM2003	20 MHz – 4000 MHz
LNA	LiConn	LNA02004000A	200 MHz – 4000 MHz
Gain Block	Mini-Circuits	ZX60-83LN-S+	500 MHz – 8000 MHz
RSA	Tektronix	RSA507A	9 kHz – 7500 MHz

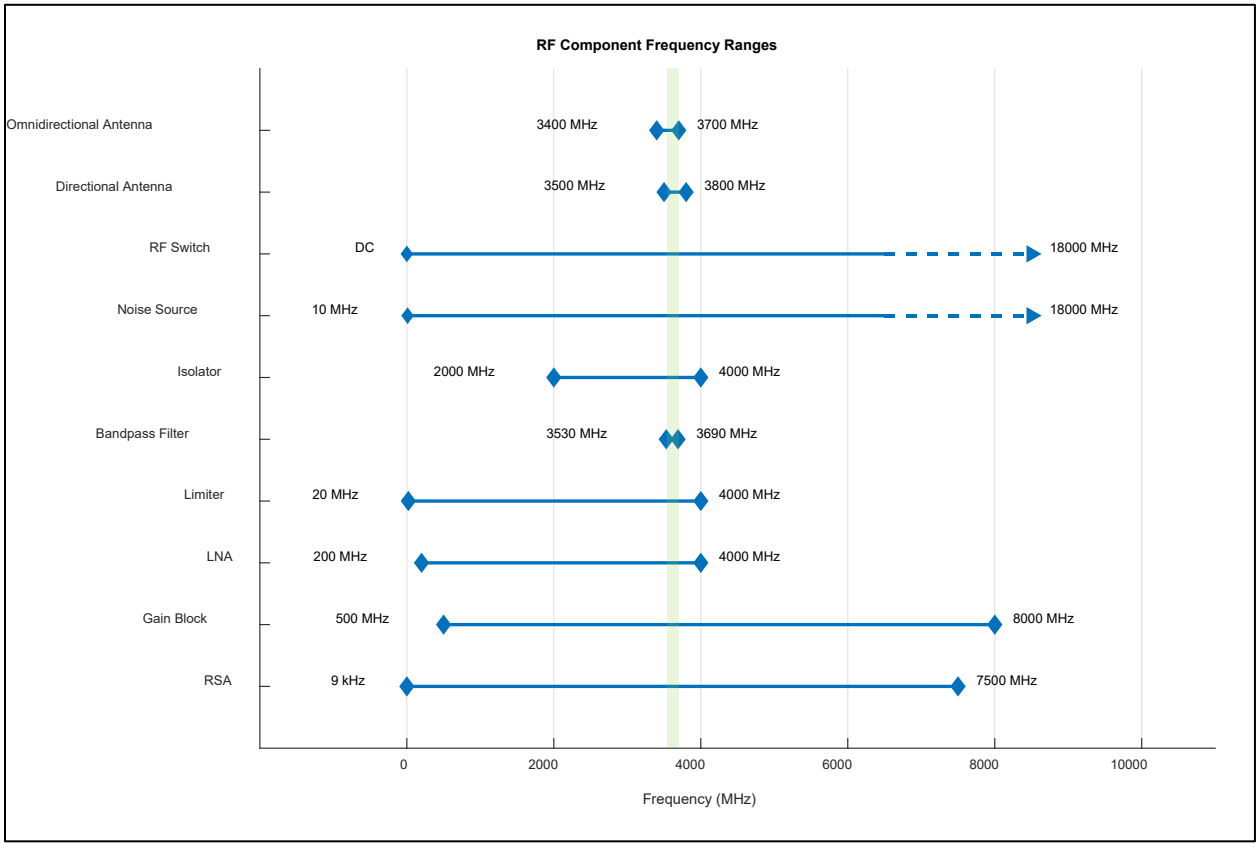

Figure A-1. Sensor RF Component Operating Frequency Ranges

The only components that limit operation to the CBRS band are the bandpass filter in the preselector and the external antennas. By replacing the filter and choosing different antennas, the sensor could be configured to operate anywhere between 2000 MHz and 4000 MHz. The lower frequency limit could be further reduced to 500 MHz by additionally replacing the isolator.

Further adaptation to other frequency bands is still possible, but would require more substantial changes possibly including the LNA, limiter and other components.

Appendix B Abbreviations and Acronyms

Term	Definition
ADC	Analog-to-Digital Converter
CBBT	Chesapeake Bay Bridge-Tunnel
CBRS	Citizens Broadband Radio Service
CBSD	Citizens Broadband Radio Service Device
CW	Continuous Wave
DANL	Displayed Average Noise Level
DPA	Dynamic Protection Area
ENR	Excess Noise Ratio
FCC	Federal Communications Commission
FFT	Fast Fourier Transform
GMM	Green Mountain Mesa
HU	Hampton University
IQ	In-phase and Quadrature
LNA	Low Noise Amplifier
LTE	Long-Term Evolution
NASCTN	National Advanced Spectrum and Communications Test Network
NEMA	National Electrical Manufacturer's Association
NIST	National Institute of Standards and Technology
NIT	Norfolk International Terminal
NTIA	National Telecommunications and Information Administration
P1dB	1 dB compression point
PDF	Portable Document Format

Term	Definition
RF	Radio Frequency
RSA	Real-Time Spectrum Analyzer
SEA	Sharing Ecosystem Assessment
SPDT	Single-Pole Double-Throw
SPU	Signal Processing Unit
TEC	Thermoelectric Cooler
UPS	Uninterruptible Power Supply
USB	Universal Serial Bus

NOTICE